Component Modeling for Fire Behavior of Shear Tab Connections

James A. Gordon and Erica C. Fischer

ABSTRACT

During a building fire scenario, the behavior and capacity of gravity connections can significantly contribute to the integrity of steel-framed building structures. Because gravity connections are subjected to axial and flexural force demands and have a limited rotational capacity due to large beam rotations during a fire scenario, a connection model is needed to simulate their behavior when using analytical models to simulate the behavior of a steel structure in fire. This study develops a component model for shear tab connections at ambient and elevated temperatures in the opensource finite element program, OpenSees, to further enable the use of OpenSees for simulating steel structures in fire, although the developed component model is not limited to implementation within OpenSees. The developed component model is benchmarked against experimental tests of isolated connections and a structural assembly with shear tab connections subjected to mechanical and thermal loads. Through benchmarking, it is shown that (1) the developed component model could be used to simulate connection behavior during a fire scenario and (2) simulating the ductility of connections and connecting components due to damage is critical when simulating the behavior of shear tab connections exposed to fire.

Keywords: component model, connections, OpenSees, steel structures in fire.

INTRODUCTION

Previous research and building fires have demonstrated the critical role of gravity connections in the stability of steel-frame structures during a fire. Gravity frame connections are susceptible to failure during a fire due to the effects of elevated temperatures, fire-induced load demands, or a combination of the two. Because floor beams provide bracing to gravity columns, the failure of beam-to-column connections can lead to column buckling during a fire, which in turn can lead to the partial or full collapse of a building.

During a fire, the increasing temperatures of structural steel components lead to the reduction of material strength and stiffness and imposed forces and deformations due to thermal expansion (Figure 1) (Burgess et al., 2012; Liu et al., 2002; Liu et al., 2019). Structural steel mechanical properties (strength and stiffness) degrade with increasing temperatures. In addition, as structural steel floor beams are heated, the thermal expansion coefficient increases (CEN, 2005a). Heated steel structural components of a building are also restrained by the surrounding cooler structure. This restraint imposes thermal deformations and axial forces in the beams (Burgess et al., 2012; Liu et al., 2002). Subsequently, the restraint will impose flexural and axial force demands in the connections (Liu et al., 2019). However, gravity connections are typically only designed for shear forces at ambient temperatures. Therefore, simulations that exclude the ability to quantify the flexural and axial force demands can underestimate the demands imposed on beams and connections throughout a fire.

Figure 1 shows the fire behavior of typical gravity connections. When gravity connections are operating at service conditions, the only significant load demands on the connection are shear forces due to gravity loading of the beams [Figure 1(a)]. During a fire, the beam expands due to thermal elongation/expansion. Thermal expansion of the beam is resisted by the surrounding structural elements, and compressive axial force develops in the connections [Figure 1(b)]. It is important to note that thermal elongation in the beam and the development of compressive axial forces in gravity connections typically occur at temperatures less than 750°F, before the mechanical properties of steel begin to degrade substantially (Burgess et al., 2012). When temperatures of the steel components exceed 750°F, the material properties (elastic modulus, Yield stress, and the proportional limit) begin to decrease. As shown in Figure 1(c), when the strength and stiffness of the beam are reduced by elevated temperatures, the beam may have large deflections and end rotations. Rotation of the beam ends can cause the bottom flange of the beam to have contact with the flange of the column it is connected to. Contact of the bottom beam flange and the column flange limits the rotational capacity of the connection, imposing large flexural

James A. Gordon, Graduate Research Assistant, School of Civil and Construction Engineering, Oregon State University, Corvallis, Ore. Email: j9882gordon@gmail.com

Erica C. Fischer, John and Jean Loosley Faculty Fellow, School of Civil and Construction Engineering, Oregon State University, Corvallis, Ore. Email: erica.fischer@oregonstate.edu (corresponding)

Paper No. 2022-06R

demands on the connection and increasing compressive forces in the beam (Hajjar et al., 2019). At this point during the fire, the gravity connection designed for only shear force demand does not behave as an idealized pin. As the gas temperatures in the compartment decrease in the cooling phase of the fire, the temperatures of the steel components also decrease, and axial tension demands develop in the connections [Figure 1(d)]. Due to these behaviors, gravity connections can be subjected to axial force (compressive and tensile), shear force, and flexural demands during a fire and allow only limited rotation of the beam ends.

This research focused on simulating the behavior of shear tab connections during a fire using a component model in OpenSees (Mazzoni et al., 2006). Specifically, the goal of this study was to develop a component model for shear tab connections at ambient and elevated temperatures through (1) reviewing previous literature on the development of component models for shear tab connections and comparing and discussing previously developed component models for the application of simulating shear tab connections subjected to fire scenarios; (2) identifying appropriate component models to use to simulate shear tab connection behavior in fire and develop the component models within the open-sourced FE program, OpenSees; and (3) benchmarking the developed component models at ambient and elevated temperatures against experimental data. While these objectives are accomplished through the use of the FE program, OpenSees, the results of this research can be applied to other FE programs.

BACKGROUND ON USING COMPONENT MODELS TO SIMULATE SHEAR TAB CONNECTIONS

General Overview of Previous Work

Rex and Easterling (2003) developed an analytical method that could approximate the force-deformation (F-δ) behavior of bolt bearing at ambient temperature based on experimental data and finite element (FE) models. However, the empirical parameters used by Rex and Easterling are only applicable at ambient temperatures; therefore, their component model was not directly evaluated in this study.

Sarraj (2007) further developed the work of Rex and Easterling (2003), resulting in a component model for shear tab connections at elevated temperatures. The bolt bearing component of the Sarraj model used the same analytical expressions for initial stiffness and F-δ behavior as Rex and Easterling but calibrated some of the equation constants to be temperature-dependent variables. The analytical expression and the temperature-dependent variables used

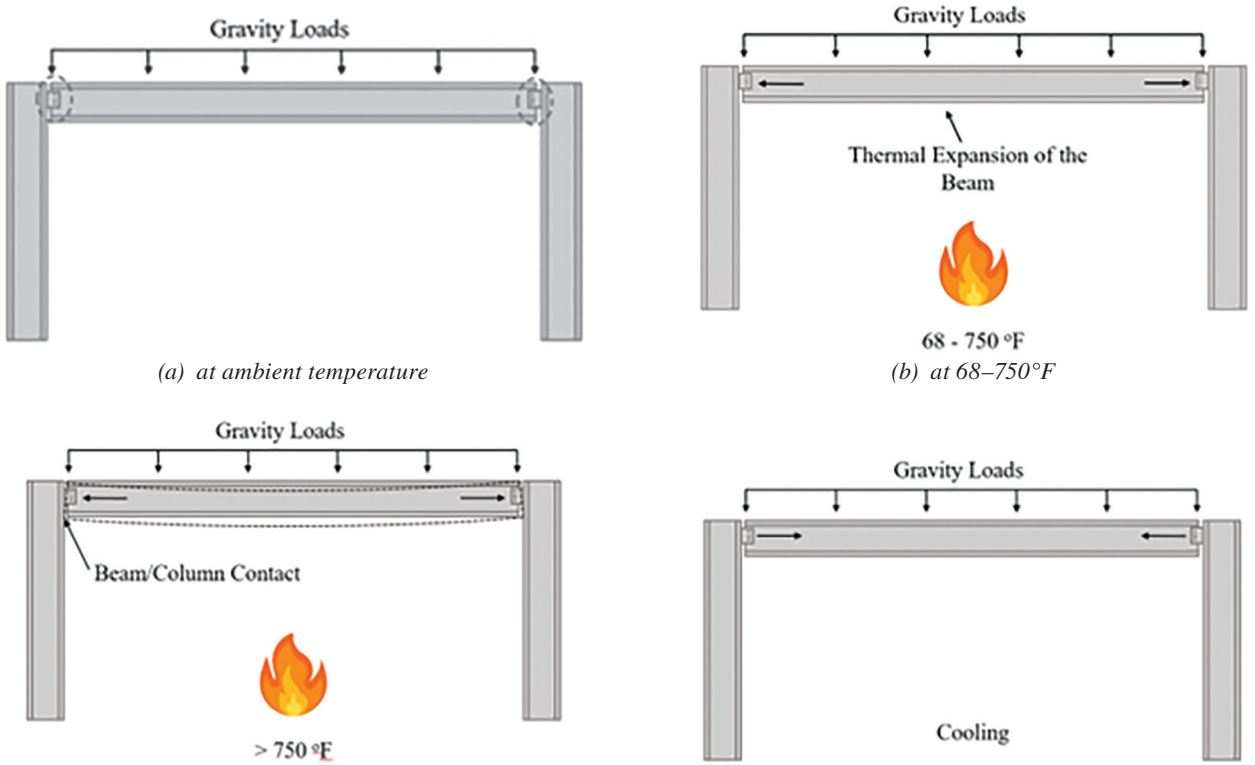

(a) at ambient temperature

(b) at 68–750°F

(c) at a temperature greater than 750°F

(d) cooling from elevated temperatures

Fig. 1. Demands and behavior of gravity connections during a fire scenario.

by Sarraj to approximate bolt shear behavior consisted of a modified Ramberg-Osgood expression that was fitted to data obtained by a series of FE analyses. After assembling the components into a component model within ABAQUS (Smith, 2009), the component model was benchmarked against a detailed FE model and test data from Wald et al. (2006).

Sadek et al. (2008) developed a component model for shear tab connections to simulate a steel beam with a composite metal deck. The component model developed by Sadek et al. (2008) consisted of bolt components and a concrete contact component. The stiffness for the bolt components was derived from the definition of rotational stiffness given by FEMA 355D (2000). While Sadek et al. calculate the limit states of the bolt components based on the observed capacities of the connecting elements, component stiffness is dependent on assumed connection stiffness instead of the observed stiffness of the connecting elements. Because the component model developed by Sadek et al. does not develop F-δ relationships based on observed behavior of the individual connecting elements, it will not be explored further in this study.

The load-deformation response for bolt bearing, bolt shear, and friction developed by Sarraj (2007) were used, validated, or modified by several researchers in subsequent studies. Yu et al. (2009) validated the bolt shear portion of the component model developed by Sarraj against a series of experimental tests. The results of the experiments were used to modify the post-peak behavior of the bolts in shear to simulate the appropriate ductility of bolts in shear at elevated temperatures.

Taib and Burgess (2011) implemented the component F-δ relationships developed by Sarraj (2007) with modified post-peak behavior representing the ductility in bolt shear failure observed by Yu et al. (2009). Taib and Burgess simplified the component F-δ curves into trilinear curves and incorporated nonsymmetrical tension and compression behavior to the bolt bearing component to account for the lack of tearout failure when the bearing components are loaded in compression.

Agarwal and Varma (2014) modified the bolt bearing and bolt shear component definitions developed by Sarraj (2007) to include post-peak behavior and account for component ductility at elevated temperatures. In addition, Agarwal and Varma added a gap element to the component model to account for the axial and rotational stiffness of the connection when the gap between the beam and column closes and the bottom flange of the beam is in bearing against the column. However, the modifications in post-peak behavior made by Agarwal and Varma assumed ductile failure of bolt shear and bolt bearing components to be initiated at a deformation of one-half the bolt diameter, regardless of the temperature. At temperatures less than 750°F, bolt shear fracture has been exhibited as a brittle failure mode.

Koduru and Driver (2014) added vertical spring components representing plate yielding and plate fracture to a component model that combined the bolt shear component developed by Sarraj (2007) and the bolt bearing component developed by Rex and Easterling (2003). In the bearing component developed by Koduru and Driver, the compressive capacity of the component is increased to account for bolt bearing failure instead of edge tearout, and the tensile capacity of the component is governed by the edge tearout. The model developed by Koduru and Driver assumes that ductile failure is initiated when the deformation is equal to half of the edge distance such that the resistance of the bearing component decreases linearly until it has zero resistance at a deformation equal to the end distance. Additionally, Koduru and Driver noted that ignoring bolt slip in the connection resulted in a 67% overestimate of peak tensile force.

Weigand (2017) developed a component model for a single plate shear tab connection with pretensioned bolts at ambient temperature for use under cyclic loading. To incorporate damage during cyclic loading, Weigand included bolt hole damage due to bearing into the component model. Because the connections considered in this study do not have pretensioned bolts, the analytical expressions developed by Weigand for component behavior are not directly compared against the other component constitutive models presented in this study. However, the consideration of bolt hole damage during load reversal is applicable to shear tab connections subjected to fire scenarios.

Weigand et al. (2018) developed a bolt shear component model using experimental testing and analytical models. Analytical models were fit to experimental data using the methodologies described in Peixoto et al. (2017). Because the constitutive model developed by Weigand et al. is highly empirical, it is limited to the range of specimen types and temperatures considered in the experimental investigation performed by Peixoto.

Xie et al. (2018a, 2018b) used detailed FE models to perform a parametric study on bolt bearing and bolt shear components to derive F-δ relationships that considered the effects of different geometric variabilities of connections. From the findings of the parametric FE study on bolt shear behavior, Xie et al. (2018b) developed a modification to the Eurocode 3 (CEN, 2005a) equation for bolt shear capacity and implemented this change into the bolt shear component model. The bolt bearing, bolt shear, and friction components were then combined to create a component model that was validated against the experimental tests performed by Yu et al. (2009).

Hajjar et al. (2019) developed a single analytical expression derived by mathematically combining component stiffnesses to calculate the response of the connection at different "stages" throughout the fire. A component representing the contact between the bottom flange of the beam

and the flange of the column was developed with a stiffness equal to the axial stiffness of the bottom flange of the beam. Because Hajjar et al. considered only a linear stiffness and did not incorporate considerations for component failure, the component definitions for bearing and bolt shear are not compared with other component models presented in this study.

Additional research has been performed to validate the component modeling approach for flexible end-plate connections. Some of the individual components and methodologies used in the flexible end-plate connection models are relevant to shear tab connection models. Silva (2001) proposed an analytical component-based procedure for modeling steel end-plate connections where the F-δ curves of the components are simplified to be bilinear. Silva classified components as either very ductile, moderately ductile, or brittle. Consequently, the post-peak F-δ behavior assigned to the components was based on the ductility category in which they are placed. Hu et al. (2009) developed a component model for flexible end-plate connections that incorporated a component to represent the contribution of a fillet weld in tension to the overall connection behavior. Hu and Engelhardt (2014) and Fischer et al. (2018) performed isolated connection tests to experimentally quantify the F-δ behavior of connections at steady-state temperatures. The tests performed by Hu and Engelhardt included a beam section and shear tab connection, while the tests performed by Fischer et al. used lap spliced joints.

Kurikova et al. (2022) developed a component model for fillet welds to aid in the design of welded joints using a component-based finite element method (CBFEM). Kurikova et al. defined the welds to have a bilinear F-δ and a plastic strain limit of 5% of the effective throat thickness of the weld. Through comparison of the analytical model developed by Kurikova et al. to data from experimentally tested longitudinal and transverse welds, it was shown that a plastic strain limit of 5% of the weld thickness is conservative for design. However, a plastic strain limit may be used to reflect the deformation recorded at weld failure during experimental tests.

Comparison of Component Models Developed

Analytical Models for Bolt-Shear Components

The bolt shear capacity within bolt shear component F-δ models developed by previous researchers is consistent between constitutive models and matches the bolt shear strength per the AISC *Specification* (2016). However, the amount of incorporated ductility varied among the available models (Figure 2) compared using a ¾-in.-diameter ASTM F3125/3125M, Gr. A325 bolt. Sarraj (2007), Weigand et al. (2018), and Xie et al. (2018b) considered the bolt in shear to fail suddenly when the force was equal to the ultimate bolt shear capacity. The models developed by Xie et al. (2018b) and Sarraj reached the ultimate bolt shear capacity before ¼ in. (6 mm) of deformation (approximately

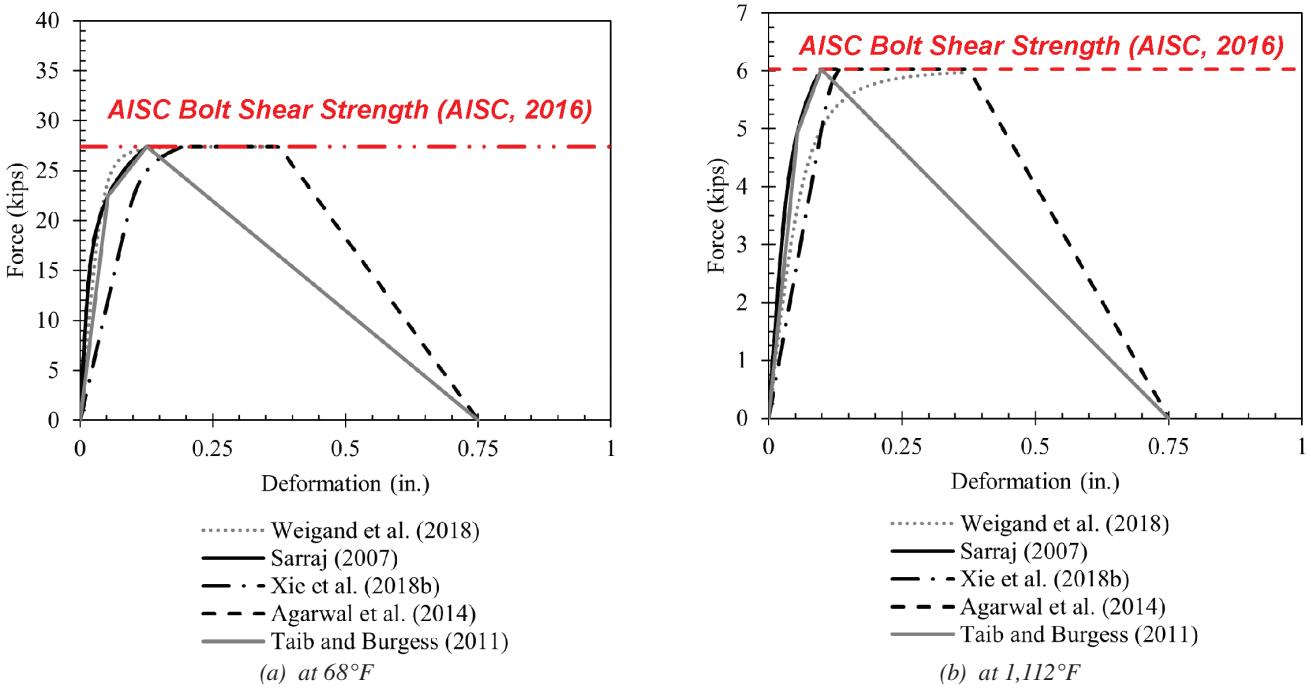

Fig. 2. Comparison of bolt shear models for a ¾-in.-diameter bolt with an ultimate stress of 140 ksi.

one-third of the bolt diameter, d_b) at ambient and elevated temperatures. However, the model developed by Weigand et al. demonstrated that larger deformations (about ⅜ in. or $d_b/2$) are achieved before the bolt shear capacity is reached and failure occurs. The model developed by Taib and Burgess (2011) considered the bolt to fail when it reaches its ultimate capacity such that the axial force capacity linearly decreases until there is zero resistance once the deformation is equal to the bolt diameter. Agarwal and Varma (2014) specified that the bolt resisted a force equal to the ultimate bolt shear capacity until the deformation was equal to half of the bolt diameter. At this point, the resisting force of the bolt in shear decreased linearly until it reached a value of zero at a deformation equal to the diameter of the bolt. In this way, Agarwal and Varma accounted for the ductility during the peak and post-peak portions of the F-δ relationship, and Taib and Burgess only accounted for ductility in the post-peak region of the F-δ relationship.

Experimental investigations (Yu et al., 2006; Peixoto et al., 2017), have shown that at temperatures greater than approximately 750°F, bolts in shear have additional ductility before and after they reach their ultimate deformation capacity. However, at ambient temperature, bolts in shear are less ductile and exhibit sudden failure (Yu et al., 2006; Peixoto et al., 2017). The ductility incorporated into the bolt shear components developed by Agarwal and Varma (2014) and Taib and Burgess (2011) is consistent with findings from experimental studies of bolts in shear at elevated temperatures but does not represent observed bolt behavior at temperatures less than 750°F. In contrast, the component models that did not consider ductility (Xie et al., 2018b; Sarraj, 2007) are consistent with observed bolt behavior at lower temperatures but do not well represent observed bolt behavior at temperatures greater than 750°F.

Analytical Models for Bolt Bearing Components

Bolt bearing component definitions were inconsistent in considering failure criteria and post-peak behavior. Although there is agreement in the literature that bolt bearing is a ductile failure mechanism, the amount of ductility incorporated within bolt bearing component models varies. Some bolt bearing components (Hajjar et al., 2019; Rex and Easterling, 2017; Sadek et al., 2008; Sarraj, 2007; Taib and Burgess, 2011; Weigand, 2017; Xie et al., 2018a, 2018b; Yu et al., 2009) had infinite ductility. For others (Agarwal and Varma, 2014; Koduru and Driver, 2014; Sadek et al., 2008), ductile failure was assumed to be initiated after a specific deformation of the bolt holes. Additionally, some researchers have developed bolt bearing components with different post-peak behaviors in tension and compression (Sadek et al., 2008). Specifically, Koduru and Driver (2014) developed these different behaviors to account for tearout versus bearing failures.

Temperature-dependent bolt bearing component models (Xie et al., 2018a; Sarraj, 2007; Agarwal and Varma, 2014), shown in Figure 3, are compared against edge tearout capacity per the AISC *Specification* (2016) at 68°F and 1,112°F, respectively (red dashed lines). The bolt bearing component derived by Xie et al. (2018b) was approximately 17% and 19% less than the strength calculated using the AISC *Specification* at 68°F and 1,112°F, respectively. The ultimate resistance approximated by the analytical model for bolt bearing derived by Sarraj (2007) was within 3% of the calculated edge tearout capacity.

The bolt bearing models proposed by Sarraj (2007) and Xie et al. (2018a) incorporated ductile post-peak behavior that gradually decreased after the ultimate capacity of the bolt bearing component was reached. The bolt bearing model proposed by Sarraj had a load resistance of 0 at approximately $9d_b$. The bolt bearing model proposed by Xie et al. (2018a) had a load resistance of 0 at approximately $21d_b$. Agarwal and Varma (2014) had failure initiated at a deformation of $½d_b$, corresponding to the failure criteria given for the bolt shear component. After the initiation of failure, the resisting force of the bolt bearing component decreased linearly until it was zero at a deformation of d_b.

Analytical Models for Gap/Contact Components

Researchers have incorporated a variety of different stiffnesses and capacities for the gap/contact between the bottom flange of the beam and the flange of the column (Yu et al., 2009; Hajjar et al., 2019; Agarwal and Varma, 2014; Hu et al., 2009; Taib and Burgess, 2011). Some researchers (Yu et al., 2009; Agarwal and Varma, 2014; Taib and Burgess, 2011) defined the gap/contact component to initially have no stiffness (simulating the gap between beam flange and column) and extremely high stiffness with unlimited capacity (simulating contact of the beam flange with the column) when the deformation was equal to the distance of the gap. This approach simulates the very high rotational stiffness that is achieved when the gap closes. However, this method does not consider deformation that may occur due to local buckling of the beam bottom flange.

Hajjar et al. (2019) defined the stiffness of the contact component to be equal to the axial stiffness of the bottom flange of the beam. Hajjar et al. also reduced the area of the bottom flange of the beam by a factor of 0.7 because only 70% of the beam flange was assumed to be in contact with the column flange. Hu et al. (2009) defined the gap/contact component to have a contact initial stiffness defined by the yielding of the column web instead of the beam flange. As shown in Figure 4, for a 42 ft W18×35 beam attached to a W12×106 column, the stiffness of the gap component approximated by the Hu et al. model is 777 kip/in., and the stiffness approximated by the Hajjar et al. model is 215 kip/in.

The stiffnesses obtained from using the Hu et al. (2009) and Hajjar et al. (2019) models for the same beam and column sizes are significantly different as shown in Figure 4. The Hu et al. model produces a relatively high stiffness (slope of the line in Figure 4), which may overestimate the stiffness of the contact between the beam flange and column stiffness if applied in a model that does not already consider damage, such as yielding, of the connected beam. Conversely, the Hajjar et al. model may overestimate the ductility of beam-to-column contact by only considering a portion of the beam cross section to be contributing to axial stiffness when contact occurs because of the lower stiffness the model produces (slope of the line in Figure 4).

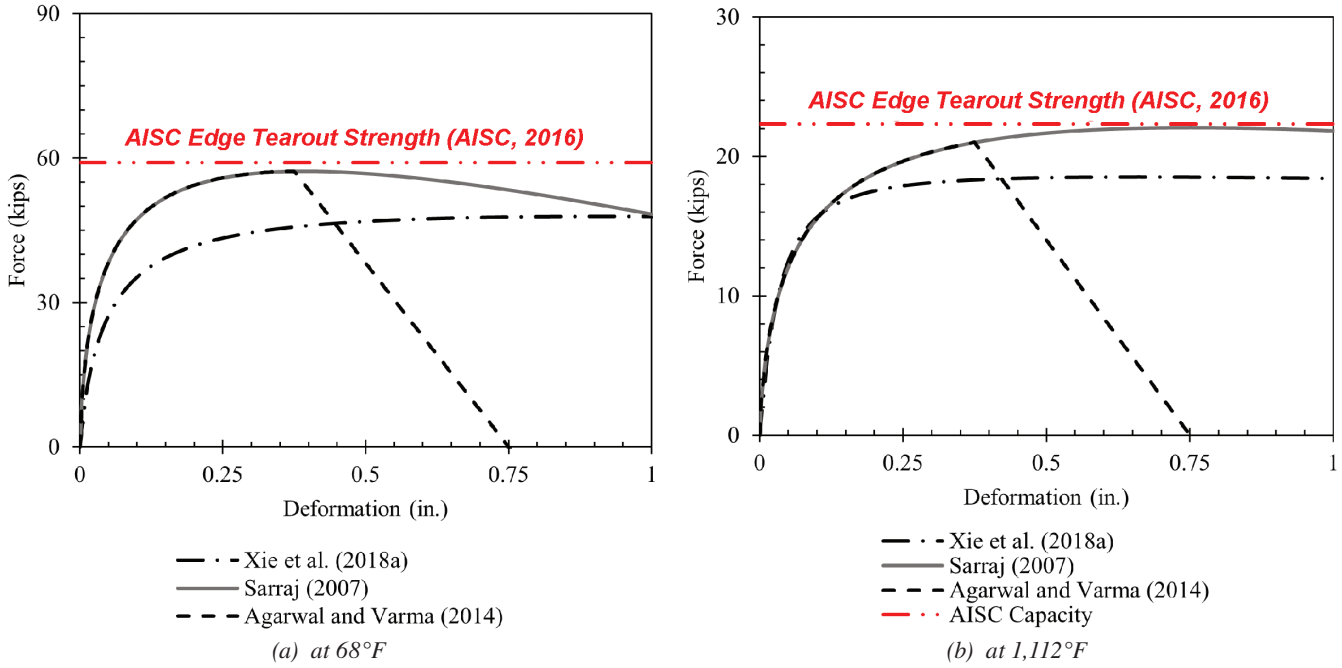

(a) at 68°F (b) at 1,112°F

Fig. 3. Comparison of bolt bearing models for a ¾-in.-bolt bearing on a 7/16-in.-thick plate with a yield stress of 50 ksi and ultimate stress of 70 ksi.

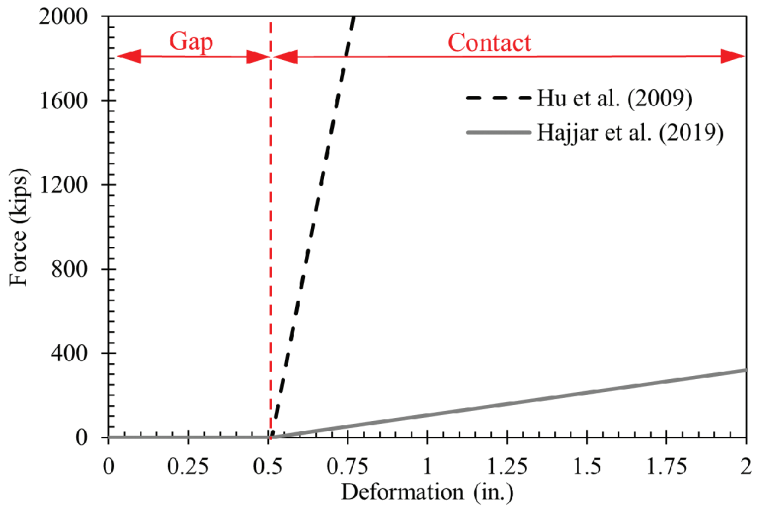

Fig. 4. Comparison of gap/contact components.

Analytical Models for Weld Components

Because the fillet welds attaching the shear tab to the column are extremely stiff and are typically designed to have a higher capacity than the other connecting elements, the weld component was often ignored in component models for shear connections. Although some researchers included weld components in their component models, very little validation has been done to test the weld component behavior. Koduru and Driver (2014) defined a weld component with a F-δ relationship defined by Lesik and Kennedy (1988). Hu et al. (2009) defined a weld component to have a maximum capacity and retention factors defined by Eurocode 3 (CEN, 2005a) with an ultimate deformation equal to 20% of the effective throat thickness of the weld, resulting in a linear F-δ relationship. Sadek et al. (2008) considered only the capacity, defined by the AISC *Specification* (2016), of the weld in the formulation of the component model and assumed it has infinite stiffness so that the deformation of the welds did not contribute to the component behavior. Kurikova et al. (2022) developed a weld component for use in design that conservatively estimated the plastic strain limit of the component to be 5% of the thickness of the weld.

Component Model Development

Component models have been utilized in many different scenarios where the behavior of gravity connections is of interest. Although the individual components of the connections are defined similarly because they represent the behavior of similar physical components, the development of a component model is dependent on its desired application. One method used by previous researchers to assemble a component model was to combine the individual springs into a single analytical expression or spring to represent the connection behavior (Hajjar et al., 2019; Taib and Burgess, 2011). This method was useful when a component model was used to account for connection stiffness and strength, but the performance of each individual component was not considered. Another method used to assemble the component model was to define each component as an individual spring that is located at the location of the connecting element that they represented (Agarwal and Varma, 2014; Hu et al., 2009; Koduru and Driver, 2014; Sadek et al., 2008; Sarraj, 2007; Weigand, 2017; Xie et al., 2018a, 2018b; Yu et al. 2009). This method resulted in a model that could be easily updated to reflect changes in geometric and material parameters and allowed the researchers to track individual component behavior. Researchers also developed component models of connections that have a combination of combined springs and single springs that represented the components. Weigand (2017) combined components located at the bolt hole (bolt bearing on the beam web, bolt bearing on the plate, and bolt shear) in series and then located a combined spring at the location of each bolt.

MODELING METHODOLOGIES FOR THE DEVELOPMENT OF A COMPONENT MODEL IN OPENSEES

This section summarizes the modeling methodologies for the development of a component model to simulate the behavior of shear tab connections subjected to fire scenarios. The component models in this study were developed in OpenSees (Mazzoni et al., 2006), but the methodologies utilized are applicable for use with other finite element programs. Individual component constitutive models were developed to represent the behavior of each active component in the connection assembly and the associated damage or failure modes. The components were then assembled into a component model in OpenSees. The developed component model was benchmarked against experimental data.

Identification of Active Components

Active components refer to the individual components of the connection whose deformation, resistance, and/or strength contributes to the behavior of the connection. As shown in Figure 5, for a typical shear tab connection, the active components include the shear behavior of the bolts, the bolt bearing on the beam web, the bolt bearing on the shear tab, the gap/contact between the bottom flange of the beam and the flange of the column, and the weld connecting the shear tab to the column flange. Friction between the components can be considered as an active component, but its effects are often considered to be minor. Therefore, friction was ignored in this study.

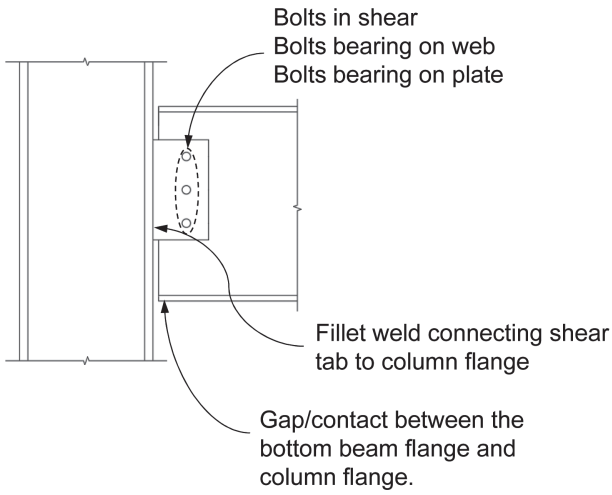

Fig. 5. Active components for a typical shear tab connection.

Component Constitutive Models

The behavior of the individual component springs was developed using the previous research presented earlier. Modifications were made to the component models developed by previous researchers to reflect observations reported from experimental investigations. The following sections provide an overview of force-deformation component models for each of the active components of the connections. The force-deformation plots shown in Figures 6 through 9 were developed for specific connection geometries provided within the captions of the figures. These plots will change with varying connection geometries.

Bolt Shear Component

Bolt shear behavior was modeled using the F-δ relationship proposed by Sarraj (2007). This component model for bolt shear was selected to simulate bolt shear behavior for a temperature range of 68°F to 1,472°F and any bolt type where F_u, E, and F_y were known. The F-δ relationship of the bolt component defined by Sarraj (2007) was calculated through four equations:

$$\Delta = \frac{F}{k_{v,b}} + \Omega\left(\frac{F}{F_{v,rd}}\right)^6 \tag{1}$$

$$F_{v,rd} = R_{f,v,b} f_{u,b} A \tag{2}$$

$$k_{v,b} = \frac{kGA}{d_b} \tag{3}$$

$$G = \frac{E}{2(1+\nu)} \tag{4}$$

where Δ is the relative bolt deformation, F is the force in the connection corresponding to Δ, $F_{v,rd}$ is the bolt shear strength (Equation 2), $f_{u,b}$ is the ultimate stress of the bolt material, $k_{v,b}$ is the bolt shearing stiffness (Equation 3), $R_{f,v,b}$ is a temperature-dependent strength reduction factor, Ω is a temperature-dependent curve fitting parameter, G is the shear modulus (Equation 4), ν is Poissons ratio, E is the elastic modulus, d_b is the diameter of the bolt, and A is the cross-sectional area of the bolt. Values for $R_{f,v,b}$ and Ω are tabulated in Sarraj (2007).

The Agarwal and Varma (2014) modifications were adopted to account for additional ductility, post-peak behavior of the bolts in shear, and bolt slip. Although Agarwal and Varma proposed modifications to account for post-peak ductility for all temperatures (including ambient temperature), bolt shear failure is brittle at ambient temperature. To account for brittle bolt shear failure at ambient temperature, the bolt shear component developed in this study loses all force resistance after reaching a deformation of half the bolt diameter (d_b/2) when the temperature is less than 750°F (Piexoto et al., 2017; Yu et al., 2009). The proposed model by the authors used a modified deformation at which the maximum resistance of the bolt occurred from d_b to ¾ d_b to reflect the post-peak behavior observed during experimental testing by others (Hu and Engelhardt, 2014; Fischer et al., 2018). The resulting F-δ relationship for bolt shear is presented in Figure 6 for temperatures of

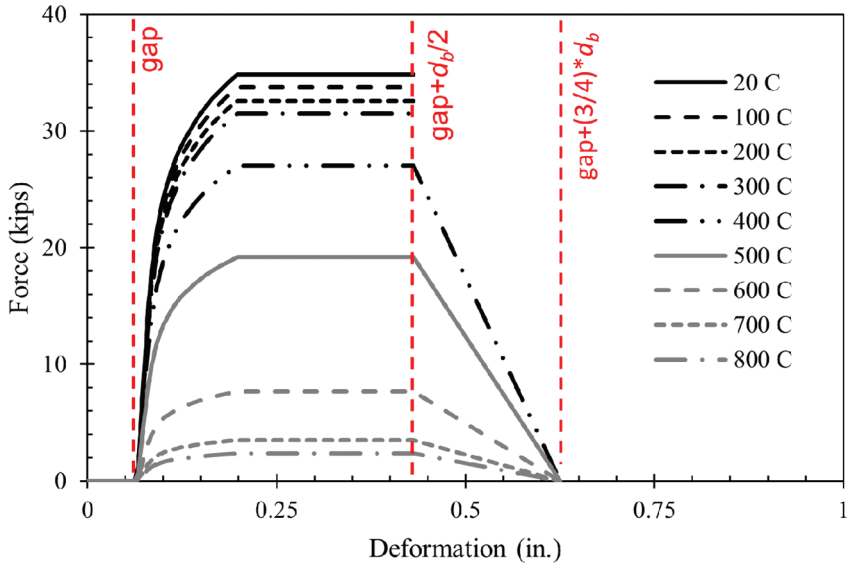

Fig. 6. Bolt shear component F-δ *relationship, for a ¾-in.-diameter bolt with an ultimate stress of 140 ksi, from Sarraj (2007) with modifications from Agarwal and Varma (2014) and experimental data.*

68°F to 1,472°F. The modification used by Agarwal and Varma specifies that the bolts retain their maximum shear capacity until the bolt reaches a deformation $d_b/2$. After the bolt reaches a deformation of $d_b/2$, the resistance of the bolt decreases linearly so that the capacity of the bolt is zero when the deformation is equal to $¾d_b$.

The bolt shear component model proposed by Sarraj (2007) was also modified to account for bolt slip. Bolt slip can occur in the connection when clear distance exists between the bolt and the edge of the bolt hole when the connection is constructed. To account for bolt slip, the connection was assumed to have deformation without any applied force for a deformation equal to the difference between the radius of the bolt hole and the radius of the bolt (assumed to be 1/16 in). In OpenSees, a small amount of stiffness was added to the portion of the F-δ curve representing this behavior to avoid singularity.

Bolt Bearing Components

Bolt bearing behavior was modeled using the F-δ relationship proposed by Sarraj (2007) with modifications for failure initiation and post-peak ductility. The F-δ relationship of the bolt bearing component defined by Sarraj was calculated through Equations 5 through 11.

$$K_i = \frac{1}{\frac{1}{K_{br}} + \frac{1}{K_b} + \frac{1}{K_v}} \tag{5}$$

$$K_{br} = \Omega t F_y \left(\frac{d_b}{25.4}\right)^{0.8} \tag{6}$$

$$K_b = 32Et\left(\frac{e_2}{d_b} - 0.5\right)^3 \tag{7}$$

$$K_v = 6.67Gt\left(\frac{e_2}{d_b} - 0.5\right) \tag{8}$$

$$\frac{F}{F_{b,rd}} = \frac{\psi\Delta'}{\left(1+\Delta'^{0.5}\right)^2} - \phi\Delta' \tag{9}$$

$$\Delta' = \Delta\beta\frac{K_i}{F_{b,rd}} \tag{10}$$

$$F_{b,rd} = \frac{e_2}{d_b} f_u d_b t \tag{11}$$

where K_i is the initial stiffness of the bolt bearing component; K_{br} is the bearing stiffness; K_b is the bending stiffness; K_v is the shearing stiffness; Ω, ψ, and ϕ are temperature-dependent curve fitting parameters; e_2 is the distance from the edge of the bolt hole to the edge of the plate in bearing; Δ' is the normalized deformation; Δ is the hole elongation; F is the bearing force; $F_{b,rd}$ is the bearing capacity of the plate; f_u is the ultimate stress of the bearing material; and β is a steel correction factor (taken as 1.0 for typical steels).

The modifications proposed by Agarwal and Varma (2014) were adopted to account for failure due to tearout in tension. The ductile post-peak behavior of the bolt bearing component developed by Agarwal and Varma corresponded to the bolt shear post-peak behavior. Therefore, the bolt bearing component developed in this study was defined to have a deformation of $¾d_b$ instead of d_b when there is zero resistance to conservatively reflect the post-peak ductility of the bolt shear component. This proposed component model used within the work summarized in this paper did not consider different F-δ relationships in tension and compression. This was a conservative approach for bolt bearing components loaded in compression and allowed for easier implementation into OpenSees. As shown by the F-δ relationship of bolt bearing components presented in Figure 7, the bolt bearing component model proposed by Sarraj (2007) was employed until the bolt bearing component reached a deformation of $d_b/2$. Afterward, the resistance of the bolt bearing component decreases linearly such that at a deformation of $¾d_b$, the resistance of the bolt bearing component is zero. Temperature-dependent retention factors for plate and web mechanical properties were utilized (CEN, 2005a; AISC, 2016).

Gap/Contact Component

The proposed gap/contact component F-δ relationship shown in Figure 8 has zero stiffness when deformation is less than the distance between the bottom beam flange and the column flange. After the gap/contact component has a deformation equal to the distance of the gap, the gap/contact component has a very high stiffness representing the beam flange in contact with the column flange. The stiffness during contact proposed by Hu et al. (2009) was adopted to give a high level of contact stiffness and because the axial stiffness of the beam, which is captured by the Hajjar et al. (2019) gap/contact component, is considered within the formulation of the beam element in this study. In addition to the gap/contact component developed by Hu et al., a modified definition of the gap/contact component model will be evaluated for cases where there is potential for local buckling of the supported beam. As shown in Figure 8, the modified gap/contact component defines the behavior of the component after contact to be elastoplastic. The yielding behavior of the modified gap/contact component accounts for damage to the beam by limiting the amount of force that can be transferred through the beam-to-column contact to the yield strength of the bottom flange of the beam (AF_y), where the yield strength is temperature-dependent.

Weld Component

The weld component was defined to incorporate a load capacity corresponding to the capacity of the weld as calculated by the AISC *Specification* (2016) and a deformation capacity consistent with the findings from Kurikova et al. (2022). The *F*-δ relationship increased linearly until the force was equal to the capacity of the weld as calculated by the AISC *Specification*. The maximum deformation of the weld was assumed to be 10% of the effective throat thickness of the weld. The deformation capacity of the weld component was chosen to reflect the deformation at failure of experimentally tested, transversely loaded fillet welds while still incorporating the conservatism employed by Kurikova et al. Welds are very stiff and brittle with little deformation before failure and no post-peak ductility. Therefore, welds can be considered active components when they are at risk of failure, but if the welds have sufficient capacity to resist the load demands placed on the connection, they contribute very little to the overall connection behavior and need not be included.

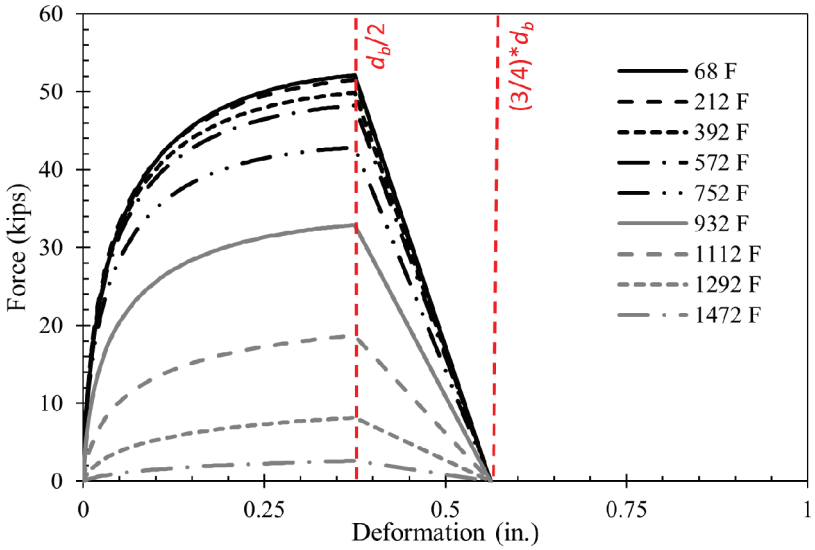

Fig. 7. Bolt bearing component F-δ *relationship for a ¾-in.-diameter bolt with an ultimate stress of 140 ksi.*

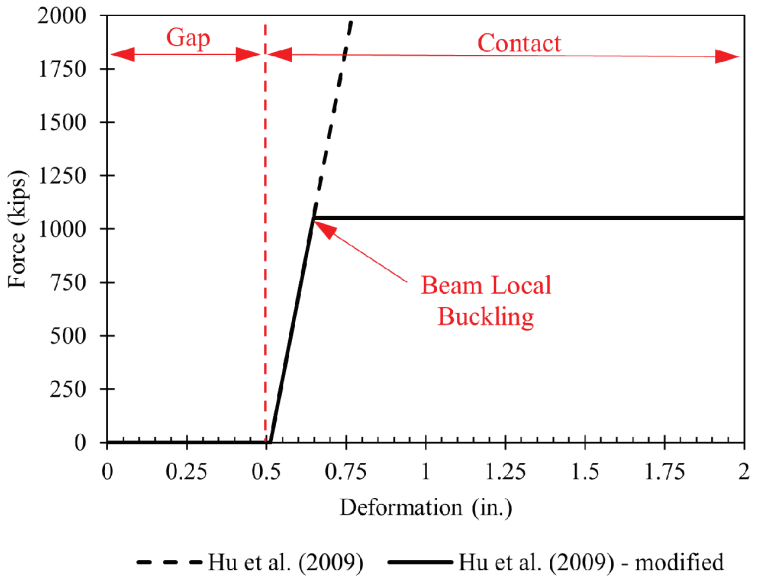

Fig. 8. Proposed gap/contact component F-δ *relationship for a W18×35 beam with a yield strength of 50 ksi.*

Assembly of OpenSees Component Model

The components were assembled into a component model within OpenSees. One node was created to represent the top of the column, and another node was created at the same location to represent the end of a beam. Nodes were then created such that each component could be placed at a vertical location corresponding to the location of the component they represented. A representation of the component model is presented in Figure 9. The F-δ relationships for the connection components at each bolt (bolt shear, bolt bearing on the shear tab, and bolt bearing on the beam web) were placed in series and combined prior to inputting the data into OpenSees, such that a single component could be defined at the location of each bolt (Figure 9 in blue). The resulting component used to simulate bolt shear, bolt bearing on the shear tab, and bolt bearing on the beam web will now be referred to as the bolt component. The gap/contact component F-δ curve was assigned at the bottom of the bottom flange (Figure 9 in purple). The weld component was discretized into a set of eight components where each component represented approximately 1 linear in. of the weld. As shown in Figure 9, the components were connected with rigid elements to the beam or column node. The components have only axial stiffness, and the end node for the beam is restrained to have the same vertical translation as the corresponding column node. In this way, the component model developed in this study only considers failure of the connection due to imposed axial force and moment demands and assumes loading in shear will not cause failure or damage within the connection throughout the fire.

In OpenSees, multilinear and hysteretic uniaxial materials were used to define the F-δ relationship for the bolt component. A multilinear material was used to create a backbone curve that more closely aligned with the nonlinearity of the calculated backbone curve. The hysteretic material is used to account for load reversal in the bolt component and allowed for the updating of temperature-dependent mechanical properties when fire loading is transient. As shown in Figure 10, seven points were used to capture material nonlinearity when a multilinear material was used in OpenSees. When a multilinear material was used to define the bolt component, a *MinMax* material was used to prevent reloading after the load-carrying capacity of the bolt component was zero at a deformation of $¾d_b$. A hysteretic material limited the definition of the backbone curve to three points. When a hysteretic material was used to model the bolt component, the first point on the backbone curve was selected to be at a location corresponding to two-thirds of the effective yield stress and one-fifth of the effective yield strain to simulate the initial stiffness of the bolt component. The next two points on the hysteretic backbone curve were the effective yield point and the point of failure initiation as depicted in Figure 10. A *MinMax* material was used to define failure for the hysteretic backbone curve after the maximum strain was reached. The gap/contact component was created using a multilinear uniaxial material with a very small initial stiffness until the deformation is equal to the distance of the gap. The weld component F-δ relationship was created in OpenSees using a *MinMax* material that referenced an elastic uniaxial material so that the weld components had a constant stiffness and a maximum strain that was 20% the effective throat thickness of the weld; the strength is calculated using the AISC *Specification* (2016), including the strength reduction factor of 0.75.

Two methods for modeling steel structures exposed to fire are available in OpenSees: (1) using preexisting OpenSees objects that were designed specifically for thermal applications, referred to herein as *OpenSeesThermal* (Jiang and Usmani, 2013; Khorsani et al., 2015; Maddalozzo et al., 2020; Walls et al., 2018), and (2) using OpenSees parameter objects to update material properties of steel in each step of the analysis to account for temperature-dependent mechanical property degradation and thermal expansion, referred to herein as *OpenSeesParameter* (Whyte et al., 2016). When

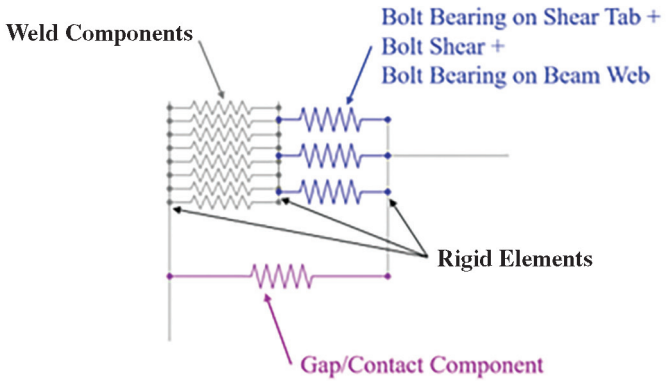

Fig. 9. Pictorial representation of the component model developed in OpenSees.

using OpenSeesThermal to simulate the behavior of an axially unrestrained beam exposed to elevated temperatures, a large axial force is developed; however, this axial force is correctly approximated to be zero when using OpenSeesParameter. The authors observed that when thermal elongation is increasing or decreasing between time steps within OpenSees, large axial forces are developed, even for axially unrestrained beams. These observations suggest that the methods of simulating a change in thermal elongation used by OpenSeesThermal results in the development of large axial forces. A more in-depth investigation is required to determine the exact origin of axial force development when using OpenSeesThermal to simulate a laterally unrestrained beam subjected to heating, which is outside the scope of this research. However, because the performance of gravity connections is sensitive to large axial loads during a fire scenario, OpenSeesParameter is used in this research in lieu of OpenSeesThermal to simulate the effects of temperature on steel connections and framing systems. A more in-depth discussion of this behavior is found in Gordon (2022).

BENCHMARKING COMPONENT MODELS AGAINST EXPERIMENTAL DATA

The OpenSees component model was benchmarked against two sets of experimental data that consisted of isolated connections tested at elevated temperatures. The component model was then used to simulate a long-span composite beam during a fire scenario to evaluate the contribution of simulating the connection behavior on the fire performance of the beam. The experimental study performed by Hu and Engelhardt (2014) was selected for benchmarking to evaluate the behavior of the components located at each bolt under pure axial load and elevated temperatures. The experimental study performed by Yu et al. (2009) was selected for benchmarking to evaluate the behavior of the gap/contact component and the entire component model when a combination of shear force, axial force, and bending moment is applied at ambient and elevated temperatures. The component model was then applied to simulate the behavior of a two-dimensional (2D) frame with a long-span composite beam and shear tab connections exposed to a fire scenario (Choe et al., 2019).

Isolated Connection Benchmarking: Hu and Engelhardt

Hu and Engelhardt (2014) performed a series of experimental tests to quantify the behavior of shear tab connections at elevated temperatures when subjected to pure tensile axial loading. In these tests, the connections were heated to a target temperature and then loaded monotonically until failure. The geometry of the shear tab connections tested by Hu and Engelhardt is presented in Figure 11.

The mode of failure for the specimens heated to 68°F and 750°F was bolt bearing failure of the shear tab, and the specimens heated to 932°F, 1,022°F, and 1292°F failed due to bolt shear. As the temperature increased, the capacity of the connection decreased, and larger deformations within the connection occurred. Although the specimen tested at ambient temperature had the largest ultimate deformation, very little post-peak ductility was present for specimens heated to 68°F and 750°F. However, post-peak ductility was observed for specimens heated to 932°F, 1,022°F, and 1,292°F.

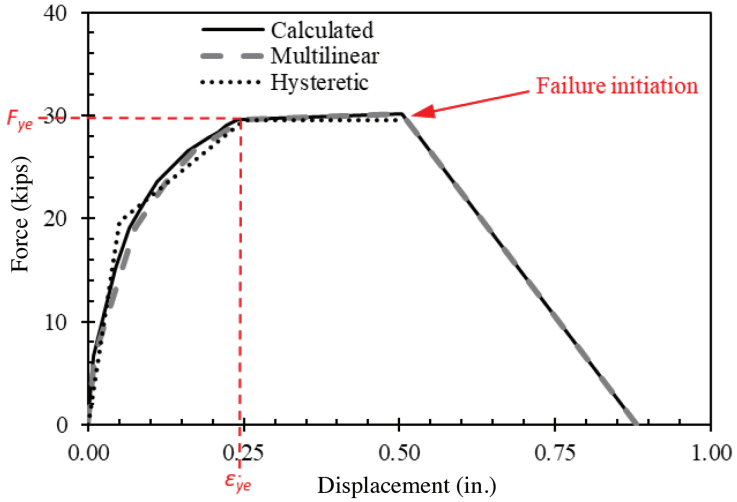

Fig. 10. Example of the simplified F-δ *relationships of the bolt component with a ¾-in.-diameter bolt with a yield strength of 116 ksi bearing on a ⅜-in.-thick plate and a ¼-in.-thick web with yield strengths of 52.2 ksi.*

The component model developed to simulate the experimental tests only included the active components. Because the Hu and Engelhardt (2014) tests only subjected the specimens to pure axial loading, the connection does not rotate, and the gap/contact between the stub beam and the column was not considered to be an active component. The weld had a larger capacity than the other connecting elements, and the stiffness of the weld was extremely high. Therefore, the weld was also not considered as an active component. The bolt component used the bolt retention factors calculated by Hu and Engelhardt from the experimental data.

Results: Hu and Engelhardt

The results from the OpenSees component model are compared with the experimental results from Hu and Engelhardt (2014) graphically in Figure 12. Table 1 compares the load capacities (denoted maximum load) and the deformation recorded before the connection fails (denoted maximum deformation) observed from experimental testing and predicted by OpenSees. In the result comparisons, load capacity refers to the maximum load that was resisted by the connection, and failure is signified by a sudden loss of load-carrying capacity. The F-δ curves presented in Figure 16 show that overall, the OpenSees component model simulated the behavior of the connections tested by Hu and Engelhardt. Although there were some differences between the experimental and analytical results, the general nonlinear shape of the F-δ relationship was accurately predicted by the component model. As shown in Table 1, the error in connection capacity predicted by the component model was less than 10% for all temperatures. The errors in ultimate deformation predicted by the component model were greatest for temperatures of 68°F and 750°F (28% and 61%, respectively). While these errors demonstrate that the model was unable to predict the ultimate deformation, in both of these simulations, the ultimate load was calculated by the OpenSees model within 10% of the experimentally measured ultimate load. In addition, both of these experiments failed in bolt tearout. The errors in ultimate deformation predicted for temperatures of 932°F, 1,022°F, and 1,292°F were less than 15%.

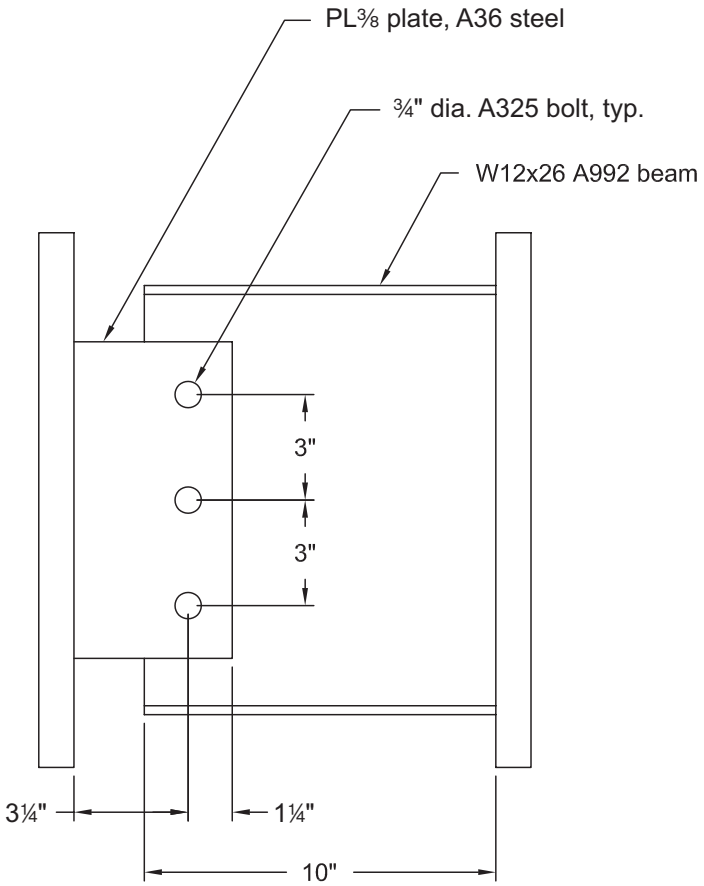

Fig. 11. Hu and Engelhardt (2014) test specimen geometry.

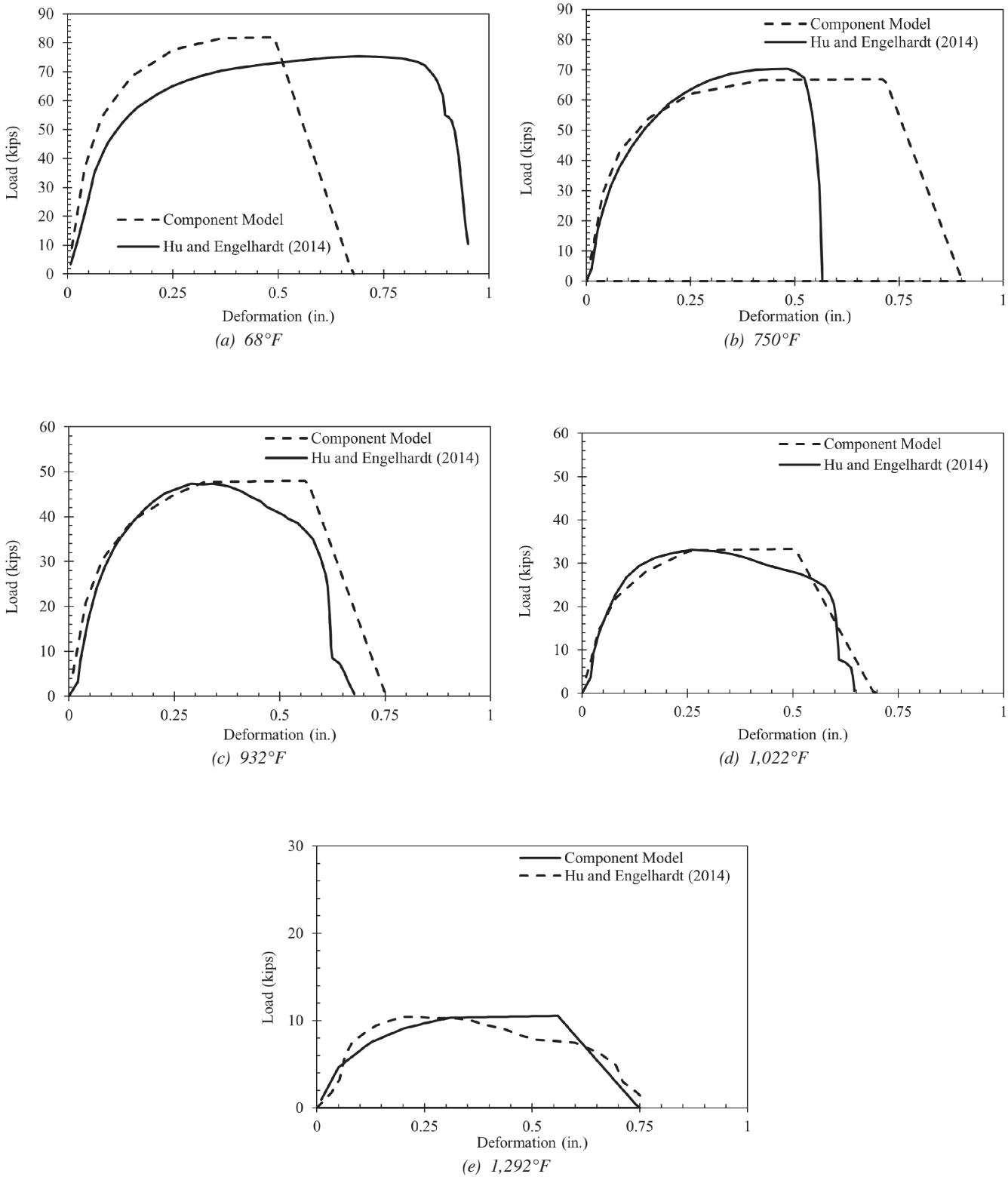

Fig. 12. Result comparison for Hu and Engelhardt (2014) tests.

Table 1. Comparison of Results Gathered from the OpenSees Component Model and Hu and Engelhardt Tests						
	Hu and Engelhardt (2014)		Component Model (OpenSees)			
Temperature (°F)	Maximum Load (kips)	Maximum Deformation (in.)	Maximum Load (kips)	Maximum Deformation (in.)	% Error Load	% Error Deformation
68	75.3	0.951	81.9	0.680	9%	28%
750	70.4	0.567	66.9	0.910	5%	61%
932	47.4	0.677	48.0	0.760	1%	12%
1022	33.1	0.646	33.3	0.700	1%	8%
1292	10.4	0.764	10.5	0.750	1%	2%

Isolated Connection Benchmarking: Yu et al.

The experimental program performed by Yu et al. (2009) evaluated the behavior of a shear tab connection subjected to elevated temperatures and a combination of axial force, shear force, and bending moment. To achieve a combination of axial force, shear force, and bending moment demands on the connection, Yu et al. applied load to the test specimens at angles of 35° and 55°. The test specimen geometry is presented in Figure 13. The force-rotation behavior recorded by Yu et al. showed that the connection has a decreasing load capacity and increasing rotational ductility as the temperature increases. All connections tests performed by Yu et al. that are used for benchmarking failed in bolt shear.

As previously described, Yu et al. (2009) developed a component model based on the component definitions proposed by Sarraj (2007). The active components included in the component model were bolt shear, bolt bearing on the plate and web, and friction between the plate and the web. To account for ductility of the bolts in shear, Yu et al. assumed the bolt component to either maintain its load-carrying capacity until a deformation equal to half of the bolt diameter ($d_b/2$) and then fail suddenly or have infinite ductility.

The retention factors for bolt shear calculated by Hu and Engelhardt (2014) were developed to simulate the experiments performed by Yu et al. (2009). Additionally, Yu et al. suggests that the bolt shear strength, F_{vrd}, be calculated as $0.692F_{ub}A_s$ instead of $0.6F_{ub}A_s$ to reflect the actual material properties of the bolt. Therefore, in the study described in this paper, the authors calculated the bolt shear strength as $0.692F_{ub}A_s$ in the proposed component model when benchmarking the proposed component model against the Yu et al. experimental tests.

Isolated Connection Benchmarking Results: Yu et al.

Figures 14 and 15 compare the test data from Yu et al. (2009) (black solid lines) with the proposed component model implemented in OpenSees (black dashed lines) developed by the authors. The results using the component model developed by Yu et al. are presented as gray dashed lines. The gray x's in Figures 14 and 15 show where failure occurs in the Yu et al. component model when the bolt component is considered to fail suddenly at a deformation of $d_b/2$; however, as seen from the testing data, that point does not always correspond with the peak load. In Table 2, the load capacities (denoted maximum load) and the deformation that occurred at the load capacity (denoted maximum rotation) are recorded.

At the beginning of the experimental tests, the bolts were not bearing against the shear tab or the beam web, allowing for rotation to occur with little resistance. Because the starting distance between the bolts and the shear tab and web edges are unknown and vary between experimental tests, the initial bolt slip was estimated for each test based on the experimental data. The estimated bolt slip was incorporated into the results of the simulation performed by the authors consistent with the methodologies used for the component model benchmarking performed by Yu et al. (2009). As the bolts came into contact with the beam web and shear tab, the stiffness of the connection increased until failure occurred. In the experimental tests and each simulation, the connection began to lose load-carrying capacity after the top bolt or the top and middle bolt failed (Yu et al. 2009). In the ambient tests, bolt shear failure resulted in a sudden loss of load-carrying capacity, after which some load transfer was regained as the middle bolt reached its maximum capacity and failed. However, the connections tested at elevated

temperatures exhibited a more gradual loss of load-carrying capacity. The component model implemented in OpenSees (developed by the authors) simulated the change from brittle to ductile failure as temperature increased; however, the component model developed by Yu et al. did not account for post-peak behavior and, therefore, could not simulate the ductile failure at elevated temperatures.

The numerical results presented in Table 2 show that the error in maximum load predicted by the component model implemented in OpenSees (developed by the authors) was equal to or less than 20%, except for the case where the load angle was 35° and the connection was heated to 1202°F (the error for this case was 31%). The errors in maximum connection rotation were less than 20% when temperatures exceeded 68°F. The close correlation between experimental and component model results demonstrated the accuracy of the OpenSees component model in predicting connection behavior.

Discussion on Benchmarking against Isolated Connection Experimental Studies

The results from benchmarking the component model against isolated connection tests show that the component model developed in OpenSees can simulate connection behavior and predict connection capacity at ambient and elevated temperatures. The agreement of results for the Hu and Engelhardt (2014) tests demonstrated the behavior of the components located at each bolt (bolt shear, bolt bearing on the beam web, and bolt bearing on the shear tab) when subjected to a purely axial load. The agreement of results for the Yu et al. (2009) test demonstrated the behavior of the gap/contact component and the overall connection behavior when subject to a combination of shear force, axial force, and bending moment at elevated temperatures. The comparison of results obtained from the component model developed by Yu et al. and the component model

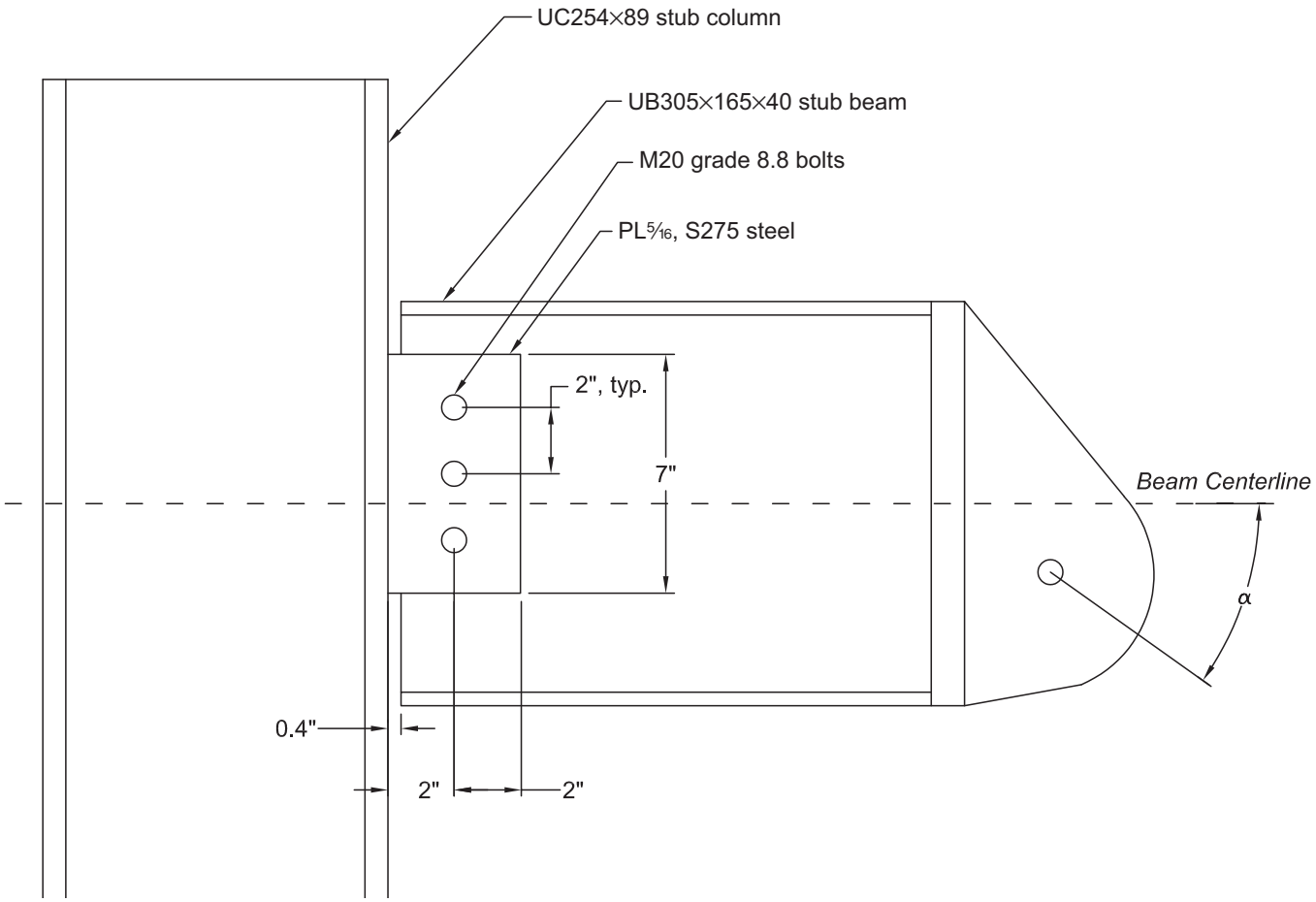

Fig. 13. Yu et al. (2009) test specimen geometry.

Table 2. Comparison of Results Gathered from the OpenSees Component Model and Yu et al. (2009) Tests						
Load Angle = 35°						
	Experimental Results		**Component Model (OpenSees)**			
Temperature (°F)	**Maximum Load (kips)**	**Maximum Rotation (deg)**	**Maximum Load (kips)**	**Maximum Rotation (deg)**	**% Error Load**	**% Error Rotation**
68	41.44	7.85	40.64	6.76	2%	14%
842	18.96	5.99	17.53	6.02	8%	1%
1022	8.66	7.02	9.11	5.79	5%	18%
1202	4.32	7.31	5.66	5.96	31%	18%
Load Angle = 55°						
	Experimental Results		**Component Model (OpenSees)**			
Temperature (°F)	**Maximum Load (kips)**	**Maximum Rotation (deg)**	**Maximum Load (kips)**	**Maximum Rotation (deg)**	**% Error Load**	**% Error Rotation**
68	32.89	11.09	29.19	9.26	11%	16%
842	15.93	6.30	14.76	6.02	7%	4%
1022	7.77	6.56	7.73	5.79	1%	12%
1202	4.03	6.27	4.74	5.96	18%	5%

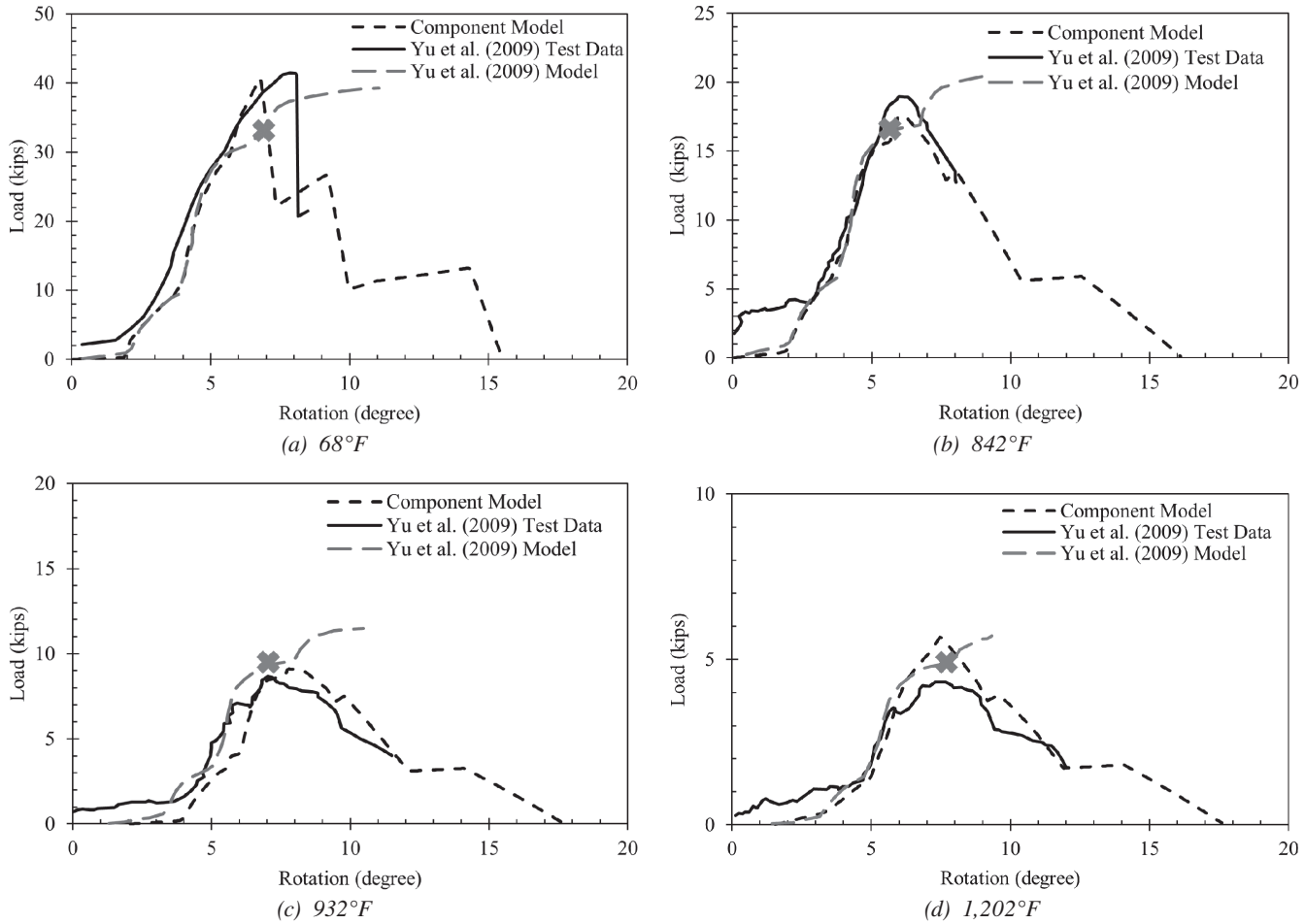

Fig. 14. Result comparison for Yu et al. (2009) tests with a load angle of 35°.

implemented in OpenSees highlights the importance of defining failure criteria for individual components when simulating the post-peak behavior of connections in fire.

The significant errors (greater than 20%) in maximum deformation at temperatures of 68°F and 760°F that were present when simulating the Hu and Engelhardt (2014) experiments indicate that the model did not accurately simulate the ductility of the connection when bolt tearout occurred. Percent errors were also high when predicting the maximum load in the Yu et al. (2009) experiments when the temperature was 1,202°F. To mitigate these errors and improve the developed component model, additional research is necessary to develop and incorporate an analytical model for bolt tearout failure that better represents observed bolt tearout failure in shear tab connections.

NIST Composite Beam Tests: Choe et al.

The component model implemented in OpenSees and benchmarked again Hu and Engelhardt (2014) and Yu et al. (2009) was then used to simulate a 2D frame consisting of a composite beam with shear tab connections (Choe et al., 2019). The test assembly consisted of a W18×35 steel beam with 6.25-in.-deep concrete on metal deck that included a 3-in.-deep metal deck (Figure 16). The beams were connected to W12×106 columns that were fixed to the strong floor in the National Fire Research Laboratory (NFRL) at the National Institute of Standards and Technology (NIST). To provide lateral support and restraint during testing, a support lattice was constructed which braced the columns at their height and mid-height (Choe et al., 2019).

Spray-applied fire-resistive material (SFRM) was used to provide a 2 hr fire resistance rating (FRR) for the steel beam (⅝ in.) and a 3 hr FRR for the columns (1 in.). The thickness of fire protection on the connections matched that of the columns (1 in.).

This composite beam test was part of a larger investigation to examine the influence of varying simple (shear) connections used in U.S. construction practices on the

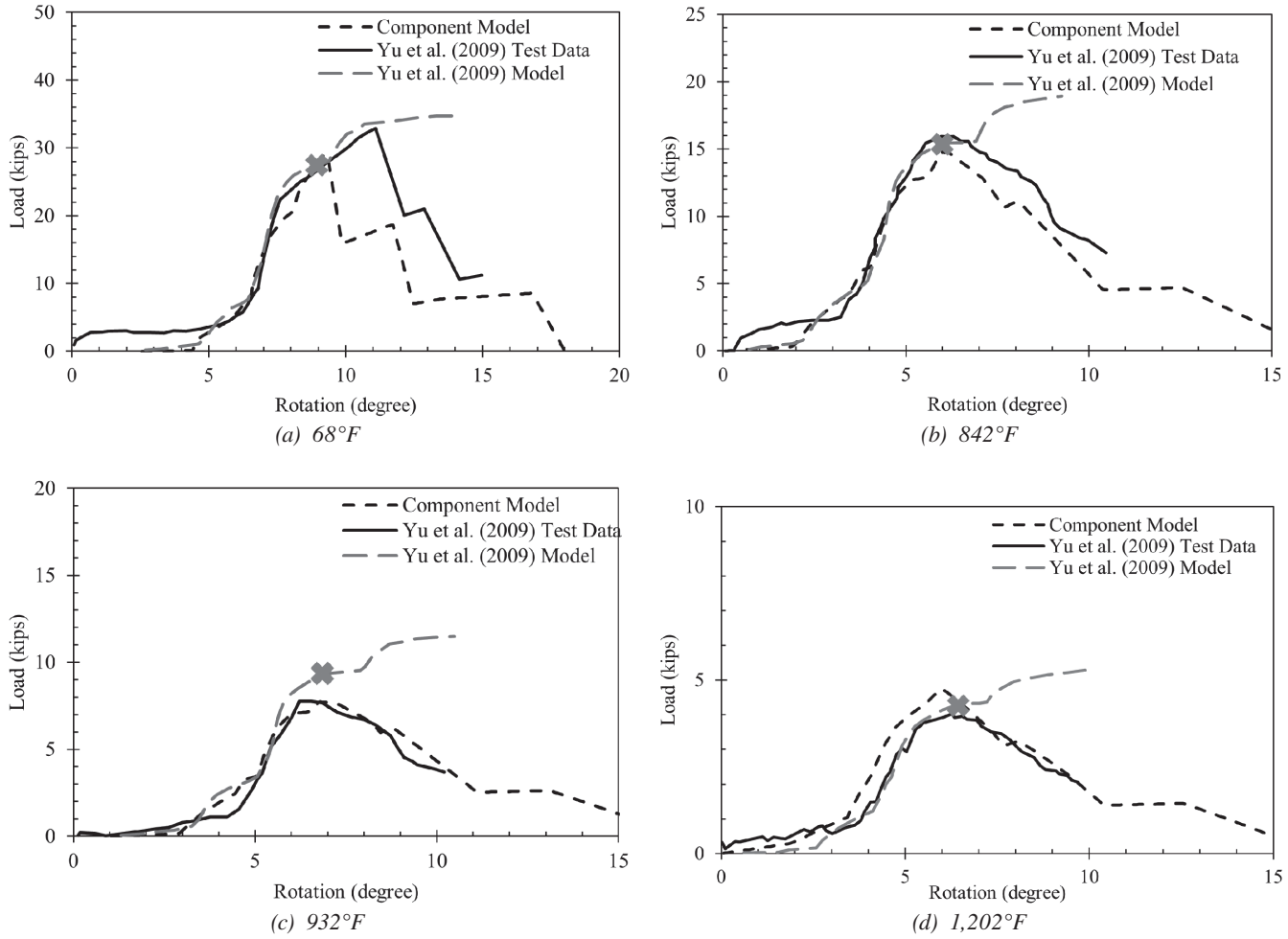

Fig. 15. Result comparison for Yu et al. (2009) tests with a load angle of 55°.

behavior of composite beams in fires (Choe et al., 2019). This research only benchmarked against the specimen that used a shear tab connection (referred to as test CB-SP in the NIST publications). This connection consisted of a 7/16-in.-thick ASTM A36/A36M shear tab connected to the column through a 5/16 in. fillet weld and connected to the beam web through three ¾-in.-diameter ASTM F3125/3125M Gr. A325 bolts (Figure 17).

The specimens tested by Choe et al (2019) were subject to a static mechanical load and a transient thermal load. Mechanical loading was first applied to the system using hydraulic actuators that loaded the composite beam through a load truss. The method for mechanical loading resulted in 6 point loads along the length of the beam. A total of 24 kips was applied (6 point loads, 4 kips each) followed by heating until the beam failed.

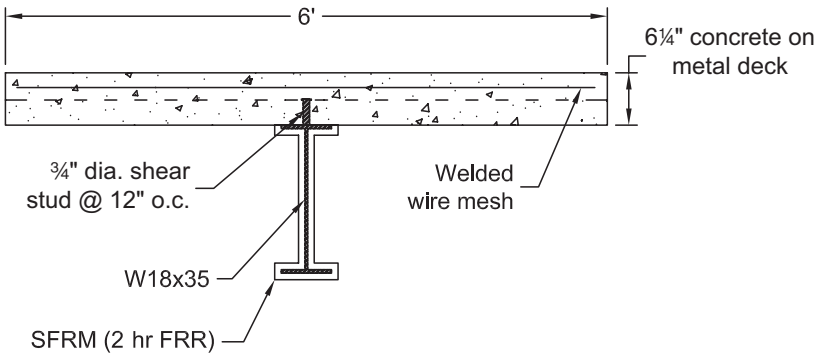

Fig. 16. NIST composite beam section.

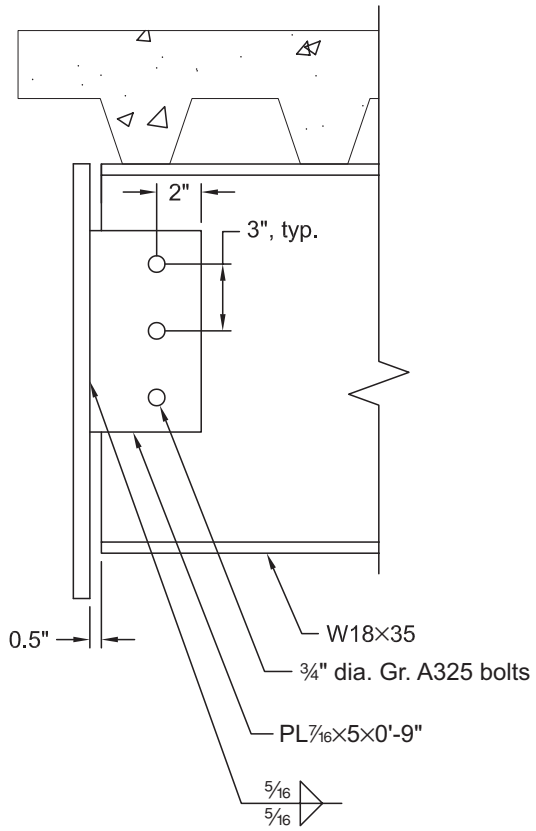

Fig. 17. Shear tab connection used in CB-SP NIST composite beam test.

After the mechanical loads were applied, thermal loading was applied to the assembly during the test by natural gas-fueled burners. The burners were used to simulate a compartment fire that was representative of a realistic yet potentially threatening fire event (Choe et al., 2019). During the heated test, the burners were set to operate at an average heat release rate of approximately 3791 BTU/s (4 MW). Once the composite beam assembly failed, the mechanical load was removed, the burners were turned off, and the compartment was allowed to cool naturally. During the test, the east beam-to-column connection failed due to weld unzipping at approximately 65 min after the beginning of the fire test, causing the collapse of the east end of the composite beam.

The locations of recording equipment used by NIST that are relevant to this study include the end rotations and the downward deflection of the beam recorded at approximately 3 ft from midspan. Temperatures were recorded during the test using Type K thermocouples at five locations along the depth of the W18×35 beam, four locations on the shear tab connection, and five locations throughout the depth of the slab. The temperatures recorded during the NIST test were input into the analytical model to determine the degraded mechanical properties of the steel beam and columns during the simulation.

To simulate the NIST assembly in OpenSees, the composite beam section was modeled using a fiber discretized section with concrete and steel material properties assigned to the appropriate fibers. This modeling approach inherently assumes that the beam is fully composite. The steel W-shape was assigned five temperature regions (one for each flange and three equally spaced in the web) corresponding to the number and location of thermocouples used in the NIST experiment. The experimentally measured temperatures of the slab were relatively low (below 392°F); therefore, the concrete slab and steel reinforcing were assumed to be unheated, and the slab was assigned a single temperature region. The columns were also modeled using a fiber discretized section that consisted of five temperature regions (one for each flange and three equally spaced in the web).

Eight connection model variations (V1–V8) were evaluated, as outlined in Table 3. V1 consisted of a purely pinned connection, which represented the behavior of the assembly when a component model is not considered. V2 included only bolt and weld components to evaluate the stiffness and overall behavior of the component model without the inclusion of a gap/contact component. V3 evaluated the forces developed in the connection when a gap/contact component is included in the component model. V4 and V5 included welds with gap/contact components and bolts with gap/contact components, respectively, to evaluate the failure behavior of the bolts and welds when modeled in combination with a gap/contact component. V6 and V7 compared the differences resulting from using a hysteretic and multilinear bolt component model and evaluated the effects of using a component model when all connection components that contribute to connection behavior are simulated. V8 demonstrated the impact of considering beam damage by including such considerations within the gap/contact component constitutive model. In all component model variations, the component force-deformation relationships were not temperature dependent because the maximum temperature recorded in the connection during the test did not exceed 513°F. At this temperature (513°F), the weld material is assumed to have no reduction in strength (CEN, 2005a), and the bolts are assumed to retain 90% of their original strength (AISC, 2016).

The test and model results that are used to define the assembly behavior are deflection near midspan (denoted VD3), connection rotation at both ends, and the axial force at the beam ends. While deflections and connection rotations were directly measured during the experiment, the axial forces at the beam ends were calculated based on the recorded strains in the bracing system (Choe et al., 2019). In the simulations, the axial forces developed at the ends of the beams and the axial forces transferred through only the connecting elements (weld and bolt components) are recorded.

During the test, the composite beam is loaded at ambient temperature. While the load is sustained, the beam is exposed to a fire scenario. Deflections began to increase as the temperature increased. During heating, local buckling occurred at the beam ends at a time of approximately 40 min. Beam buckling resulted in strain reversal and a loss of compressive axial load at the beam ends. At a time of 65 min, the beam deflected approximately 21.6 in., and weld failure occurred at the west connection. At this time, there was some additional midspan beam deflection (approximately 5.5 in.), and the west connection rotation increased significantly. After connection failure, the beam was allowed to cool naturally, the load was removed, and there was some deflection and connection rotation recovery.

Effects of Component Model Implementation into NIST Composite Beam Simulation

The benchmarked component model was implemented within a 2D frame to simulate the behavior of a composite beam with shear tab connections during a fire scenario. The beam deflection, the connection rotations, sum of forces through connecting components, and lateral force reactions at the end of the beam were recorded when using different variations of the component model (Figure 18). The midspan deflections approximated by using V1 (a pinned connection) in the analytical model are 29% lower than those recorded during the experimental test (Choe et al., 2019)

Table 3. Connection Model Variations for Benchmarking against the NIST (Choe et al., 2019) Composite Beam Test						
Connection Model Variation	Included Components				Bolt Material Type	
	Pin	Welds	Bolts	Gap/ Contact	Multilinear	Hysteretic
V1	√					
V2		√	√		√	
V3	√			√		
V4		√		√		
V5			√	√	√	
V6		√	√	√	√	
V7		√	√	√		√
V8		√	√	√*		√
* gap/contact component includes beam damage considerations						

when the west connection fails at 65 min. Initially, a tensile axial force of 36 kips is present in the beam when using V1. As the beam expands due to thermal elongation, the tensile force at the ends of the beams decreases. At approximately 35 min, tensile forces begin to increase due to the flexural yielding of the beam [Figure 18(c)]. After the mechanically applied gravity loads are removed from the beam at a time of 65 min, an axial force of less than 11 kips is developed.

The deflections and connection rotations changed by less than 20% during the duration of the test when bolt and weld components are incorporated into the proposed component model to simulate the shear tab connections (V2) as compared to a purely pinned connection (V1). Including bolt components when simulating the connection (V2) resulted in slightly larger midspan deflections (less than 1 in.) between times of 50 and 65 min as compared to a purely pinned connection (V1). Connection rotations approximated when using V2 remained within ±0.017 rad of those approximated by V1. Additionally, using a component model that considers the initial gap between the bolt and the edge of the bolt holes (V2, V5, V6) simulated the initially unrestrained displacement of the bolt components, and axial forces were not initially developed as they were when the bolt hole gap is not considered (V1, V3, V4, V7).

When a gap/contact component was included in V3 (purely pinned connection with gap/contact component) and V4 (only weld and gap/contact component), the gap between the beam and column flanges closed at approximately 35 min, and large axial forces began to develop [Figures 18(c) and 18(d)]. In V3, gap closure resulted in reduced midspan deflections, and the maximum deflection was 39% less than the experimentally measured just before connection failure. As the assembly cooled, connection rotation was recovered in the analytical model, and the gap opened at a time of approximately 117 min. When the gap closed at approximately 35 min in V4, large bending moments began to develop at the beam ends as large compressive forces were transferred through gap/contact component and large tensile forces were transferred through the weld components. At a time of 44 min, the tensile force transferred through the weld components exceeded the weld strength (190 kips calculated using the AISC *Specification*) and the welds failed. Weld failure caused nonconvergence of the analytical model signifying the loss of stability of the composite beam assembly, which is highlighted by red circles in Figure 18.

When a bolt component was used in combination with a gap/contact component with infinite stiffness (V5–V7), bolt shear failure occurred after the gap closed. The midspan deflection and connection rotation when using V5–V7 to simulate connection behavior were within 3% of one another. This indicated that the behavior of the composite beam and connection failure simulated by the component model was not sensitive to the inclusion of weld components or the different material types used in V6 (bolt material simulated as multilinear) and V7 (bolt material simulated as hysteretic). Failure of the bolts resulted in an increased rotational capacity of the connections and increased deflections compared to simulations that did not include bolt components (V1–V4). The maximum deflections of V5–V7 were within 10% of the deflection recorded right before failure during the experimental tests.

The axial forces developed in the beam ends when using V5–V7 were almost 60% greater than those approximated by Choe et al. (2019). However, when damage to the beam (i.e., local buckling at beam ends) is accounted for by limiting the amount of force transferred through the gap/contact component (V8), the axial forces are within 10% of those

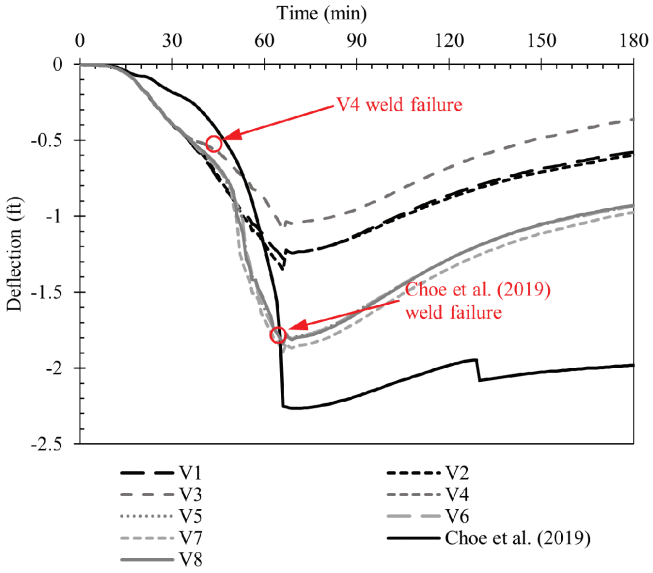

(a) VD3 deflection

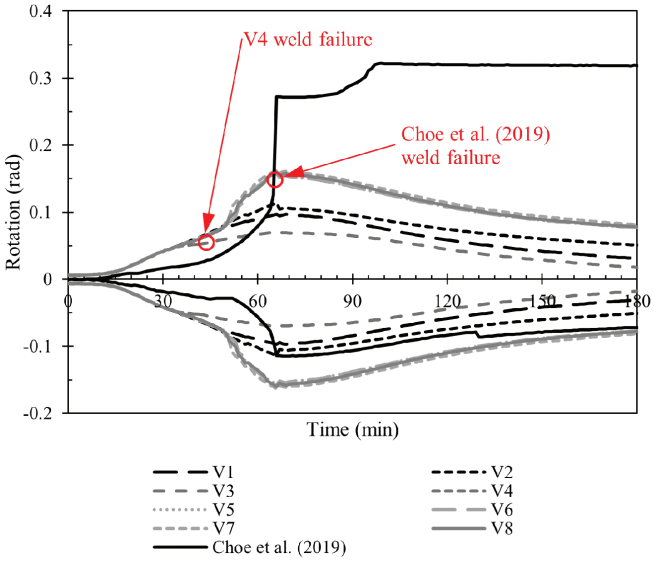

(b) connection rotations

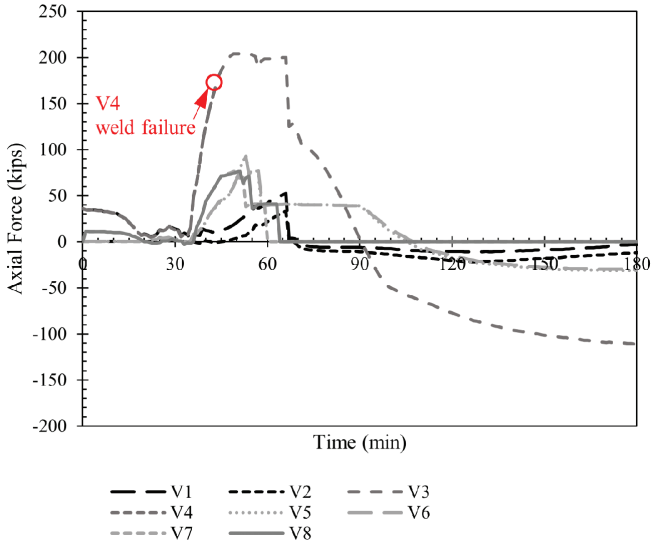

(c) sum of axial forces transferred through connecting components

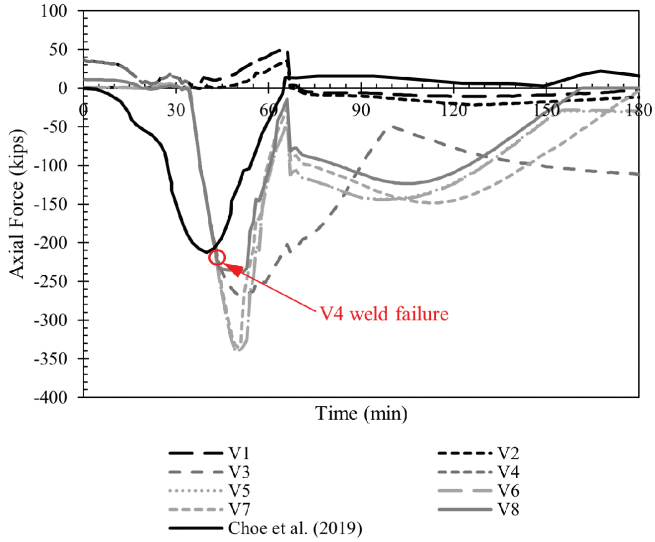

(d) axial forces at the ends of the beams

Fig. 18. Results comparison for NIST composite beam test (Choe et al., 2019).

Table 4. Summary of Results from the Simulation of the NIST Composite Beam Test (Choe et al., 2019)							
Connection Variation	Maximum Deflection (ft)	% Error Maximum Deflection	Maximum P_m (kips)	% Error Maximum P_m	Maximum P_{ce} (kips)	Maximum Connection Rotation (rad)	% Error Maximum Connection Rotation
Experimental data	–1.79	–	214	–	–	0.114	–
V1	–1.28	29%	11.0	95%	52	0.097	15%
V2	–1.36	24%	21.6	90%	33	0.114	0%
V3	–1.10	39%	267	25%	204	0.097	15%
V4	–0.55	69%	227	6%	167	0.054	52%
V5	–1.84	2%	341	59%	94	0.157	38%
V6	–1.84	3%	342	59%	92	0.157	38%
V7	–1.89	6%	335	56%	79	0.164	44%
V8	–1.84	3%	237	10%	77	0.161	41%

approximated by Choe et al. Additionally, when V8 is used, the maximum connection rotation was 40% greater than the maximum rotation recorded during experimental testing.

Discussion on Using the Component Model to Simulate Connection Behavior in a 2D Frame

Including a gap/contact component in the component model resulted in the development of large axial forces and bending moments due to beam-to-column contact. Accounting for beam damage by limiting the amount of force transferred through the gap/contact component, the component model predicted the gap/contact component to yield at a time of 44 min (4 min after local beam buckling occurred in the experimental test) and limited axial forces at the beam ends to 237 kips (10% greater than those approximated by Choe et al., 2019). Whereas, when this gap/contact component was not included, the simulation did not predict the development of compressive axial forces at the beam ends during the heating phase of the experiment (Table 4). This behavior demonstrates the importance of including the gap/contact element to simulate the fire behavior of shear tab connections and gravity beams.

Large deflections of the composite beam were able to be simulated by accounting for the ductility of the bolt components. The maximum deflections obtained when the bolt component was included in V5–V7 were within 10% of those recorded during the test. Whereas, when the bolt component was not included (V1–V4), the maximum beam deflections were within 40% of the experimental data (Table 4). However, additional research on the weld components should be performed as the OpenSees model predicted bolt shear fracture as the controlling failure mode in V2 and V5–V8, which is not consistent with the weld unzipping failure that was observed during physical testing (Choe et al., 2019). When the bolt component was not included within the component model, the OpenSees model did not predict failure of the specimen, although in cases where a weld component was included, weld fracture did occur.

SUMMARY AND CONCLUSIONS

In this study, a review of existing component models is presented and a component model for shear tab connections is developed in OpenSees. The component model is benchmarked against physical tests of isolated connections at elevated temperatures and a full-scale fire test of a long-span composite-beam assembly. Through this process, the definition of individual component behaviors, the behavior of the component model alone, and the behavior of the component model in a larger structural model were evaluated.

When modeling experimental testing of isolated connections where bolt shear was the governing failure mode, the proposed component model predicted the maximum capacity and corresponding level of ductility within 20% of the test data. When bolt tearout failure controlled, the deformations corresponding with maximum capacity were significantly higher (28% and 61%) than those recorded during experimental testing. Thus, the component model developed in OpenSees is considered to accurately approximate isolated connection behavior at elevated temperatures when subjected to axial force or a combination of axial force, shear force, and bending moment. However, additional research may be helpful in reducing modeling errors when bolt tearout is the controlling failure mode.

Using the component connection model to simulate the behavior of shear tab connections in the NIST composite

beam test (Choe et al., 2019) enabled the analytical model to simulate the development of large axial forces during the heating and cooling phases of the fire. Incorporating considerations for the ductility and damage of the connection components and structural elements was important when simulating the NIST composite beam test (Choe et al., 2019). Accounting for damage to the bolt components enabled the analytical model to simulate large beam deflections and changes in connection rotation that occurred at elevated temperatures. However, future work is necessary to account for the different failure mechanisms and associated damages of connection components loaded in tension versus compression within the model developed in this paper.

Modifications to include different compression and tension behavior would help mitigate the simulation of premature failure of connections loaded in compression. Accounting for damage to structural elements was shown to be important in approximating component failure and axial force generation. The gap/contact component definition developed in this study to account for damage to the steel beam limited forces to be within 10% of those approximated by Choe et al. (2019). Incorporating more detailed damage considerations when modeling the composite floor system may limit discrepancies between analytical and experimental results. The developed numerical modeling methodology for connections can more accurately predict isolated connection behavior at elevated temperatures when bolt shear is the governing failure mode. When simulating connection failure in the isolated connection tests (Hu and Engelhardt, 2014; Yu et al., 2009) it was shown that defining components to fail suddenly ignored the ductile failure observed at elevated temperatures (>750°F). Furthermore, to simulate the ductile failure of shear tab connections in fire it is important to define the post-peak behavior of individual components to reflect the post-peak behavior of the components observed during physical testing. Eurocode 3, Part 1-8 (CEN, 2005b) states that the deformation capacity of welds should not be considered; however, the test results of Choe et al. (2019) demonstrate that importance of weld deformation capacity throughout a fire condition as the weld deformation capacity is potentially exceeded prior to the force capacity of the welds, initiating unzipping of the weld. Further research and development of weld component models are suggested such that this damage and failure can be simulated throughout a fire scenario.

ACKNOWLEDGMENTS

This research was funded by the Pacific Earthquake Engineering Research (PEER) Center and the American Institute of Steel Construction (AISC). Any opinions, findings, and conclusions are those of the author and do not necessarily reflect the views of the sponsors. Special thanks and acknowledgement to Dr. Kevin Mackie, professor at the University of Central Florida, and Dr. Michael Scott, professor at Oregon State University, for their support of this research.

REFERENCES

Agarwal, A. (2011), "Stability Behavior of Steel Building Structures in Fire Conditions," Ph.D. dissertation, Purdue University, West Lafayette, Ind.

Agarwal, A. and Varma, A.H. (2014), "Fire Induced Progressive Collapse of Steel Building Structures: The Role of Interior Gravity Columns," *Engineering Structures*, Vol. 58, pp. 129–140.

AISC (2016), *Specification for Structural Steel Buildings,* ANSI/AISC 360-16, American Institute for Steel Construction, Chicago, Ill.

Burgess, I., Davison, J.B., Dong, G., and Huang, S. (2012), "The Role of Connections in the Response of Steel Frames to Fire," *Structural Engineering International,* Vol. 22, No. 4, pp. 449–461.

CEN (2005a), *Eurocode 3: Design of Steel Structures—Part 1–2: General Rules—Structural Fire Design*, European Committee of Standardization, Brussels.

CEN (2005b), *Eurocode 3: Design of Steel Structures—Part 1–8: Design of Joints,* European Committee of Standardization, Brussels.

Choe, L., Ramesh S., Grosshandler, W., Hoehler, M., Seif, M.S., Gross, J., and Bundy, M. (2019), "Behavior and Limit States of Long-Span Composite Floor Beams with Simple Shear Connections Subject to Compartment Fires: Experimental Evaluation," *Journal of Structural Engineering,* Vol. 146, No. 6.

FEMA (2000), "State of the Art Report on Connection Performance," FEMA-355D*,* Federal Emergency Management Agency, Washington, D.C.

Fischer, E.C., Varma, A.H., and Qiaqia Z. (2018), "Experimental Evaluation of Single-Bolted Lap Splice Joints at Elevated Temperatures," *Journal of Structural Engineering*, Vol. 144, No. 1.

Gordon, J.A. (2022), "Advancements Toward the Simulation of Steel Structures in Fire in OpenSees," Master's Thesis, Oregon State University, Corvallis, Ore.

Hajjar, M., Hantouche E.G., and El Ghor, A.H. (2019), "Shear Tab Connection with Composite Beam Subjected to Transient-State Fire Temperatures: A Rational Model for Design," *Journal of Structural Fire Engineering.* Ahead-of-print.

Hu, G. and Engelhardt, M.D. (2014), "Experimental Investigation of Steel Single Plate Beam End Connections at Elevated Temperatures," *Engineering Structures*, Vol. 58, pp. 141–151.

Hu, Y., Davison, B., and Burgess, I. (2009), "Component Modelling of Flexible End-Plate Connections in Fire," *International Journal of Steel Structures*, Vol. 9, No. 1, pp. 1–15.

Jiang, J. and Usmani, A. (2013), "Modeling of Steel Frame Structures in Fire Using OpenSees." *Computer and Structures*, Vol. 118, pp. 90–99.

Khorsani, N.E., Garlock M.E.M., and Quiel, S.E. (2015), "Modeling Steel Structures in OpenSees: Enhancements for Fire and Multi-Hazard Probabilistic Analyses," *Computers and Structures*, Vol. 157, pp. 218–231.

Koduru, S.D. and Driver, R.G. (2014), "Generalized Component-Based Model for Shear Tab Connections," *Journal of Structural Engineering*, Vol. 140, No. 2.

Kurikova, M., Vild, M., Frantisek W., Jehlicka, P., Kabelac, J., and Taras, A. (2022), "Fillet Weld Model for Component-Based Finite Element Method," AISC–EECS Workshop on Connections in Steel Structures, Coimbra, Portugal.

Lesik, D.F. and Kennedy, D.J.L. (1988), "Ultimate Strength of Eccentrically Loaded Fillet Welded Connections," *Structural Engineering,* Report 159, University of Alberta, Edmonton, AB, Canada.

Liu T.C.H., Fahad, M.K., and Davies, J.M. (2002), "Experimental Investigation of Behaviour of Axially Restrained Steel Beams in Fire," *Journal of Constructional Steel Research*, Vol. 58, pp. 1,211–1,230.

Liu Y., Huang S., and Burgess, I. (2019), "Investigation of a Steel Connection to Accommodate Ductility Demand of Beams in Fire," *Journal of Constructional Steel Research*, Vol. 157, pp. 182–197.

Maddalozzo, W. and Fischer, E.C. (2020), "Post-Earthquake Fire Performance of Steel Buildings," *17th World Conference on Earthquake Engineering*, Sendai, Japan, September 13–18.

Mazzoni, S., McKenna, F., Scott, M.H., and Fenves, G.L. (2006), *OpenSees Command Language Manual*, University of California, Berkeley, http://opensees.berkeley.edu/manuals/usermanual.

Peixoto, R.M., Seif, M.S., and Viera, L.C. (2017), "Double-Shear Tests of High-Strength Structural Bolts at Elevated Temperatures," *Fire Safety Journal*, Vol. 94, No. 8-21.

Rex, C.O. and Easterling, S.W. (2003), "Behavior and Modeling of a Bolt Bearing on a Single Plate," *Journal of Structural Engineering*, Vol. 129, No. 6, pp. 792–800.

Richard, R.M. and Abbot, B.J. (1975), "Versatile Elastic-Plastic Stress-Strain Formulation," *Journal of Structural Engineering*, Vol. 101, pp. 511–515.

Sadek, F., El-Tawil, S., and Lew, H.S. (2008), "Robustness of Composite Floor Systems with Shear Connections: Modeling, Simulation, and Evaluation," *Journal of Structural Engineering*, Vol. 134, No. 11, pp. 1,717–1,725.

Sarraj, M. (2007), "The Behavior of Steel Fin Plate Connections in Fire," Ph.D. dissertation, The University of Sheffield, Sheffield, United Kingdom.

Seif, M., Weigand, J., Main, J., Peixoto R., and Vieira L. (2018), "Shear Behavior of High-Strength Bolts at Elevated Temperatures: Testing and Formulation of Reduced-Order Model," NIST Technical Note 1978.

Silva, L.S., Santiago, A., and Real, P.V. (2001), "A Component Model for the Behavior of Steel Joints at Elevated Temperatures," *Journal of Constructional Steel Research,* Vol. 57, pp. 1,169–1,195.

Smith, M. (2009), ABAQUS/Standard User's Manual, Version 6.9.

Taib, M. and Burgess I.W. (2011), "A Component-Based Model for Fin-Plate Connections in Fire," *Application of Structural Fire Engineering*, Vol. 4, pp. 113–122.

Wald, F., Strejcek, M., and Ticha A. (2006), "On Bolted Connection with Intumescent Coatings," *Proceedings of the Fourth International Workshop "Structures in Fire—SiF*, Aveiro, Portugal, pp. 371–322.

Walls, R.S., Vilijoen, C., and Clereq, H. (2018), "Analysis of Structures in Fire as Simplified Skeletal Frames Using Customized Beam Finite Element," *Fire Technology*, Vol. 54, No. 6, pp. 1,655–1,682.

Weigand, J.M. (2017), "Component-Based Model for Single-Plate Shear Connections with Pretension and Pinched Hysteresis," *Journal of Structural Engineering*, Vol. 143, No. 2.

Weigand, J.M., Peixoto, R., Vieira Jr., L.C.M., Main, J.A., and Seif, M. (2018), "An Empirical Component-Based Model for High-Strength Bolts at Elevated Temperatures," *Journal of Constructional Steel Research*, Vol. 147, pp. 87–102.

Whyte, C.A., Mackie, K.R., and Stojadinovic (2016), "Hybrid Simulation of Thermomechanical Structural Response," *Journal of Structural Engineering*, Vol. 142, No. 2.

Xie, B., Hou, J., Xu, Z., and Dan, M. (2018a), "Component-Based Model of Fin Plate Connections Exposed to Fire—Part I: Plate in Bearing Component," *Journal of Constructional Steel Research*, Vol. 149, pp. 1–13.

Xie, B., Hou, J., Xu, Z., and Dan, M. (2018b), "Component-Based Model of Fin Plate Connections Exposed to Fire—Part II: Establishing of the Component-Based Model," *Journal of Constructional Steel Research*, Vol. 149, pp. 218–231.

Yu, H., Burgess, I.W., Davison, J.B., and Plank, R.J. (2009), "Experimental Investigation of the Behavior of Fin Plate Connections in Fire," *Journal of Constructional Steel Research*, Vol. 65, pp. 723–736.